

Along-strike extent of earthquakes on multi-segment reverse faults; insights from the Nevis-Cardrona Fault, Aotearoa New Zealand

Jack N. Williams *, Mark W. Stirling ¹, Robert Langridge ², Govinda Niroula ¹, Ashleigh Vause ¹, James Stewart ³, Andy Nicol ⁴, Ningsheng Wang ⁵

¹Department of Geology, University of Otago, Dunedin, New Zealand, ²GNS Science, Lower Hutt, Wellington, New Zealand, ³GeoSolve Ltd, 8 Pinot Noir Drive, Cromwell, New Zealand, ⁴School of Earth and Environment, University of Canterbury, Christchurch, New Zealand, ⁵School of Geography, Environment and Earth Sciences, Victoria University of Wellington, Wellington, New Zealand

Author contributions: *Conceptualization:* J.N.W., M.W.S. *Investigation:* all authors. *Formal Analysis:* J.N.W., N.W.. *Writing - original draft:* J.N.W. *Writing - Review & Editing:* M.W.S., R.L., A.N., J.S.. *Funding acquisition:* M.W.S..

Abstract Evaluating if earthquakes will rupture across fault segment boundaries is important for our understanding of seismic hazard and fault growth. However, the role of segment boundaries in reverse fault earthquakes is still unclear. Here, we combine fault mapping and trench data from the multi-segment Nevis-Cardrona Fault (NCF) in the South Island of Aotearoa New Zealand to assess if it has hosted single or multi-segment earthquakes during the late Quaternary. Two new trenches on its Nevis segment provide stratigraphic evidence for two surface rupturing earthquakes, which through Optically Stimulated Luminescence dating and OxCal modelling, are constrained to have occurred at $28.9^{+12.9}_{-9.1}$ ka and 12.8 ± 4.9 ka. The most recent event's timing is only weakly correlated to the timings of surface rupture documented in two trenches along the NCF's NW Cardrona segment. Furthermore, the $1.0^{+0.7}_{-0.3}$ m Nevis segment single event displacements we estimate would be unusually low for a ~ 85 km long NCF multi-segment rupture. We therefore surmise that late Quaternary NCF surface rupturing earthquakes did not rupture through the ~ 30 - 50° bends that link these segments. Our trench data and fault mapping also indicate lower slip rates on the Nevis segment than previous studies ($0.07^{+0.11}_{-0.04}$ mm/yr vs 0.4 ± 0.2 mm/yr).

Non-technical summary Earthquake magnitude is proportional to the length of fault rupture. It is therefore important that forecasts of future earthquakes use realistic fault lengths. However, this can be challenging as faults exhibit geometrical complexities along their length, such as bends and steps, and these complexities can impede earthquake rupture. More empirical data on how geometrical complexities influenced past earthquake ruptures is therefore required. In this study, we excavated trenches across the southern part of the Nevis-Cardrona Fault in the South Island of Aotearoa New Zealand, and from interpreting the offset of different geologic layers exposed in the trenches and dating methods, we obtained timings for its prehistoric earthquakes. We then compared these timings to previous estimates for earthquake timings on this fault's northern segment. These suggest that previous Nevis Cardrona Fault earthquakes were confined to individual segments that are bound by ~ 30 - 50° bends along its length. Our study also suggests lower fault slip rates (and hence longer earthquake interevent times) on the Nevis Cardrona Fault than previous studies (0.04-0.1 vs. 0.4 mm/yr). This result provides an improved understanding of earthquake hazards around the nearby towns of Queenstown, Wānaka, and Cromwell.

1 Introduction

The concept that faults lengthen by the coalescence of distinct segments underpins many fault growth models (Cartwright et al., 1995; Dawers and Anders, 1995; Jackson et al., 1996; Walsh et al., 2003; Amos et al., 2010; Rotevatn et al., 2019). In turn, this leads to kinematic and geometric segment boundaries that can persist even after a fault has accumulated many kilometres of displacement (King, 1986; Ellis and Dunlap, 1988; Mazzoli et al., 2005; Accardo et al., 2018). In the context of probabilistic seismic hazard analysis (PSHA), appropriate characterisation of segment boundaries is im-

portant, as they can influence whether fault sources are forecast to generate ruptures along short discrete segments or larger, but more infrequent, multi-segment or even multi-fault ruptures (Field et al., 2014; Chartier et al., 2019; Visini et al., 2020). This is particularly important for low slip rate faults and high probabilities of exceedance, where PSHA is especially sensitive to how fault segmentation is treated (Valentini et al., 2017, 2020; Williams et al., 2023)

To this end, a range of empirical data (Crone and Haller, 1991; DuRoss et al., 2016; Biasi and Wesnousky, 2016, 2017), physics-based simulators (Douilly et al., 2015; Zielke and Mai, 2023), and statistical methods (Field et al., 2014; Chartier et al., 2019; Visini et al.,

Production Editor:
Carmine Galasso
Handling Editor:
Randolph Williams
Copy & Layout Editor:
Oliver Lamb

Signed reviewer(s):
Nicholas Harrichhausen

Received:
March 14, 2024
Accepted:
September 18, 2024
Published:
October 31, 2024

*Corresponding author: jack.williams@otago.ac.nz

2020; Gerstenberger et al., 2024) have been developed to incorporate fault segmentation into PSHA. However, challenges remain when applying these concepts to reverse faults as there is a discrepancy between some studies that suggested that their earthquakes have a tendency to rupture across segment boundaries (Rubin, 1996; McCalpin and Carver, 2009; Arrowsmith et al., 2017), and historical surface rupture compilations, in which reverse fault earthquakes are no more likely to rupture across bends or gaps than strike-slip or normal faults (Biasi and Wesnousky, 2016, 2017). Resolving this question calls for more empirical data of segmentation during individual reverse fault earthquakes (e.g., Hubbard et al., 2014; Stahl et al., 2016; Patyniak et al., 2021). By combining new and existing fault mapping and paleoseismic data, the aim of this study is to evaluate whether late Quaternary surface ruptures of the Nevis-Cardrona Fault in the South Island of Aotearoa New Zealand were single segment or multi-segment events. Our results also provide new insights into strain localisation within slowly deforming fault systems, and new information for seismic hazard assessment around the rapidly growing communities and infrastructure in the nearby Queenstown-Wānaka-Cromwell region (Mackey, 2015).

2 The Nevis-Cardrona Fault

2.1 Regional tectonic setting

Within the southern South Island of Aotearoa New Zealand, ~70–90% of plate boundary motion between the Australian and Pacific plates is accommodated by strike-slip motion on the Alpine Fault and subduction of the Australian Plate at the Puysegur subduction zone (Fig. 1a; Norris and Cooper, 2001; Barnes, 2009; Barth et al., 2014). Of the remaining plate motion, 1–2 mm/yr of WNW-ESE convergence is accommodated on NNE-SSW striking range-bounding reverse faults that collectively define the Otago range and basin reverse fault province (McSaveney and Stirling, 1992; Norris, 2004; Beavan et al., 2016; Denys et al., 2016; Barrell, 2019; Griffin et al., 2022b). Slip rates on individual faults are estimated to be 0.05–1 mm/yr (Pace et al., 2005; Barrell, 2019; Griffin et al., 2022a,b; Seebeck et al., 2024; van den Berg et al., 2023; Johnson et al., 2024), which is consistent with relatively low rates of seismicity across this region (Fig. 1a; Warren-Smith et al., 2017; Todd et al., 2020; Eberhart-Phillips et al., 2022).

2.2 Fault nomenclature

It has been convention to term the set of quasi-continuous reverse fault strands that extends for 130 km from Lake Hawea to the Mataura River as the ‘Nevis-Cardrona Fault System’, and which in turn comprises the Nevis, NW (Northwest) Cardrona, and Cardrona-Hawea faults (Beanland and Barrow-Hurlbert, 1988; Kerr et al., 2000; Turnbull, 2000; Barrell, 2019; Seebeck et al., 2024; van den Berg et al., 2023). However, folding of the Waipoumou Erosion Surface and a sliver of late Cenozoic footwall sediments indicates that

there is a continuous geologic expression of faulting between the ~47° and ~30° bends that link the Nevis and NW Cardrona faults (Fig. 1b; Turnbull, 2000; Barrell, 2019). We therefore find it more appropriate to describe these structures as two segments of a single hard-linked fault. Likewise, the splay between the NW Cardrona and Cardrona-Hawea faults near Wānaka, does not necessitate that they are distinct faults (Faure Walker et al., 2021). We therefore adopt the terms ‘Nevis-Cardrona Fault’, and the Nevis, NW Cardrona, and Cardrona-Hawea segments in this study. We use the term ‘strand’ to describe different across-strike Nevis-Cardrona Fault splays (Barrell, 2019).

2.3 Geologic Setting

The Nevis-Cardrona Fault (NCF) is a west-dipping reverse fault that marks the boundary between the Otago range and basin reverse fault province and the higher elevation, steeper topography, and thickened crust of the Southern Alps (Beanland and Barrow-Hurlbert, 1988; Warren-Smith et al., 2017; Barrell, 2019; Eberhart-Phillips et al., 2022; Seebeck et al., 2024). NCF activity is thought to have initiated in the Late Miocene-Early Pliocene when angular schist clasts sourced from its uplifting hanging wall ranges first appear in its package of non-marine late Cenozoic footwall sediments (Fig. 1c; McKay, 1897; Williams, 1974; Beanland and Barrow-Hurlbert, 1988; Turnbull, 2000; Youngson et al., 2002; McDonnell and Craw, 2003). These sediments are preserved in four structurally controlled basins: Nokomai, Cardrona, and the Upper and Lower Nevis valleys (Fig. 1b). Based on the differences in elevation between these basins and their respective hanging wall ranges, the throw on the NCF varies along strike between 0.5–1.5 km (Fig. 1d; Beanland and Barrow-Hurlbert, 1988).

The Cardrona-Hawea segment represents the NCF’s northernmost extent (Beanland and Barrow-Hurlbert, 1988; Turnbull, 2000; Barrell, 2019). However, there is no evidence for post-glacial activity (i.e., since 18 ka) on this segment; instead the most recent NCF surface ruptures appear to be restricted to a NNW striking strand between the Cardrona valley and Lake Wānaka (Barrell, 2019). To the south, multiple discontinuous (<1 km long) fault scarps are identified on mid-level alluvial fans and fluvial terrace surfaces in the Cardrona valley and Crown Range (Fig. 1b; Beanland and Barrow-Hurlbert, 1988; Langridge et al., 2016; Barrell, 2019; van den Berg et al., 2023).

Between the Kawarau River valley and Doolans Saddle, the NCF passes through two prominent bends that link the NW Cardrona and Nevis segments (Fig. 1b). As this section coincides with fluvial downcutting in the Kawarau River valley (Fig. 1d), it is challenging to follow other studies (Philip et al., 1992; Jackson et al., 1996; Amos et al., 2010; Stahl et al., 2016) that use along-strike elevation profiles and drainage patterns to examine how reverse fault segments linked. Changes in the provenance of ~650 ka sediments downstream of the Kawarau River have been used to suggest this drainage pattern formed due to progressive westward headwall erosion (Bell, 1992; Craw, 2013). This could be equivo-

cal evidence for a causal link between where the Kawarau River valley formed and a displacement minima at a NCF bend; however, we cannot exclude the alternative possibility that the Kawarau River represents an antecedent drainage network.

NCF scarps are identified on mid-level alluvial fan surfaces throughout the Lower and Upper Nevis valleys along its Nevis segment (Fig. 1b; [Beanland and Barrow-Hurlbert, 1988](#); [Turnbull, 2000](#); [Langridge et al., 2016](#); [Barrell, 2019](#)). Further south, there is geologic evidence for the NCF extending into the Nokomai catchment, however, no scarps have been identified in this catchment (Fig. 1b; [Kerr et al., 2000](#)). Instead, Quaternary fault displacement in the Nokomai catchment is predominantly accommodated on the E-dipping Roaring Lion Fault ([Kerr et al., 2000](#)).

Detailed geologic mapping and 12 paleoseismic trenches on the NCF were conducted in the 1980's for the purposes of seismic hazard assessment of hydroelectric developments in the Kawarau and Clutha rivers (Fig. 1c). Results were initially disseminated in unpublished technical reports and student theses that covered different NCF segments ([Beanland, 1984](#); [Beanland and Fellows, 1984](#); [Beanland et al., 1984](#); [Beanland and Barrow, 1984a,b,c](#); [Beanland, 1985](#); [Barrow-Hurlbert, 1985](#)), and then later synthesised by [Beanland and Barrow-Hurlbert \(1988\)](#) in a comprehensive overview of late Quaternary NCF activity. From these investigations, evidence for up to four late Quaternary NCF surface rupturing earthquakes were presented. However, due to the limited range of dating techniques in the 1980's, rupture timings could only be constrained for a trench at Gibbston in the Kawarau River valley where organic sediments were present (Fig. 1c; [Beanland, 1985](#); [Beanland and Barrow-Hurlbert, 1988](#)).

More recently, surface rupture timings were constrained for the NCF's NW Cardrona segment following re-exposure, re-assessment, and Optically Stimulated Luminescence dating of sediments from a trench at Macdonalds Creek (Fig. 1c; [van den Berg, 2020](#); [van den Berg et al., 2023](#)). This study suggested that the penultimate and most recent surface ruptures inferred from the Macdonalds Creek and Gibbston trenches can be correlated ([van den Berg et al., 2023](#)). Prior to this study, the only chronostratigraphic constraint for Nevis segment surface ruptures is a radiocarbon date of $10,955 \pm 370$ calendar years before present (two standard deviation error following recalibration in OxCal using the SH20 calibration curve, [Hogg et al., 2020](#)) from a buried peat 0.8 m above the active channel of Whittens Creek, and so an upper bound for the age of the unfaulted flood plain (Fig. 2a; [Beanland and Barrow, 1984b](#); [Barrow-Hurlbert, 1985](#)). A $0.25^{+0.08}_{-0.05}$ mm/yr Nevis segment uplift rate has also been suggested based on the inference that the Nevis-Nokomai divide is currently ~ 100 m above the modern channel, and that the genetic divergence of galaxiid fish currently inhabiting these two catchments suggest the divide formed 300-500 ka ([Watters et al., 2001](#); [Craw et al., 2012](#)).

2.4 Upper Nevis valley

We focus here on the expression of the NCF's Nevis segment in the Upper Nevis valley, where the two paleoseismic trenches described in this study were excavated (Fig. 2). In this 12 km long NNE-trending intermontane basin, Torlesse Terrane-affiliated Haast Schist is mapped only on the topographically higher western side, and the boundary between it and the structurally higher Caples Terrane-affiliated Haast Schist coincides with the NCF's main strand (Fig. 2b). Hence, it has been inferred that late Cenozoic displacement on the NCF has thrust the Torlesse Terrane over Caples Terrane in the Upper Nevis valley ([Turnbull, 2000](#); [Boyce, 2002](#)). The regionally extensive late Cretaceous-early Cenozoic Waipounamu Erosion Surface has been cut into the top of the basement on the eastern side of the Upper Nevis valley ([Stirling, 1990](#); [Landis et al., 2008](#)), and there may be localized remnants of it to the west in the Tapuae-o-Uenuku/Hector Mountains ([Boyce, 2002](#)).

Within the Upper Nevis valley, a sequence of late Cenozoic sediments covers the Waipounamu Erosion Surface (Fig. 2). This sequence, which has correlative equivalents in the Lower Nevis valley and elsewhere in the Otago range and basin reverse fault province ([Williams, 1974](#); [Youngson et al., 1998](#); [McDonnell and Craw, 2003](#)), consists of Miocene fluvial conglomerates and lacustrine sediments (Manuherikia Group), Pliocene conglomerates (Schoolhouse Fonglomerate), and Quaternary gravels that underlie four sub-planar geomorphic surfaces (AF1-AF4; [Beanland and Barrow, 1984b](#); [Barrow-Hurlbert, 1985](#); [Boyce, 2002](#)). These surfaces represent alluvial fans, and they are distinguished by their relative elevation above the modern channel of the Nevis River (T0, Fig. 2). AF4 and AF3 are found only as remnants in a structural high in the centre of the valley where they have been detached from their alluvial material source to the west. AF1 is the surface of an alluvial piedmont that is found across the valley, and which in detail comprises a composite surface that has been locally incised by 1–3 m ([Beanland and Barrow, 1984b](#); [Beanland and Barrow-Hurlbert, 1988](#); [Boyce, 2002](#)).

Formation of these alluvial fans likely correspond to past glacial cycles, when the Upper Nevis valley experienced a periglacial climate, and there would have been an abundance of material for rivers to aggrade in non-glaciated areas ([Barrow-Hurlbert, 1985](#); [Boyce, 2002](#)). However, the degree to which surfaces AF1-AF4 can be individually correlated to glacial cycles in the regional Upper Clutha Glacial System is unclear ([Boyce, 2002](#); [Barrell, 2011](#)). Within the current interglacial period, the Upper Nevis valley experiences a semi-arid climate with < 1 m rainfall/year ([McSaveney and Stirling, 1992](#); [Macara, 2015](#)).

The main NCF strand, termed the Western Boundary Fault (WBF; [Beanland and Barrow, 1984a](#); [Barrow-Hurlbert, 1985](#); [Beanland and Barrow-Hurlbert, 1988](#)), runs along the western side of the Upper Nevis valley. However, no scarps have been identified on the WBF ([Beanland and Barrow, 1984a](#); [Barrow-Hurlbert, 1985](#); [Boyce, 2002](#); [Barrell, 2019](#)). By contrast, an ~ 8 km long 1–2 m high scarp, which we refer to as the Nevis strand,

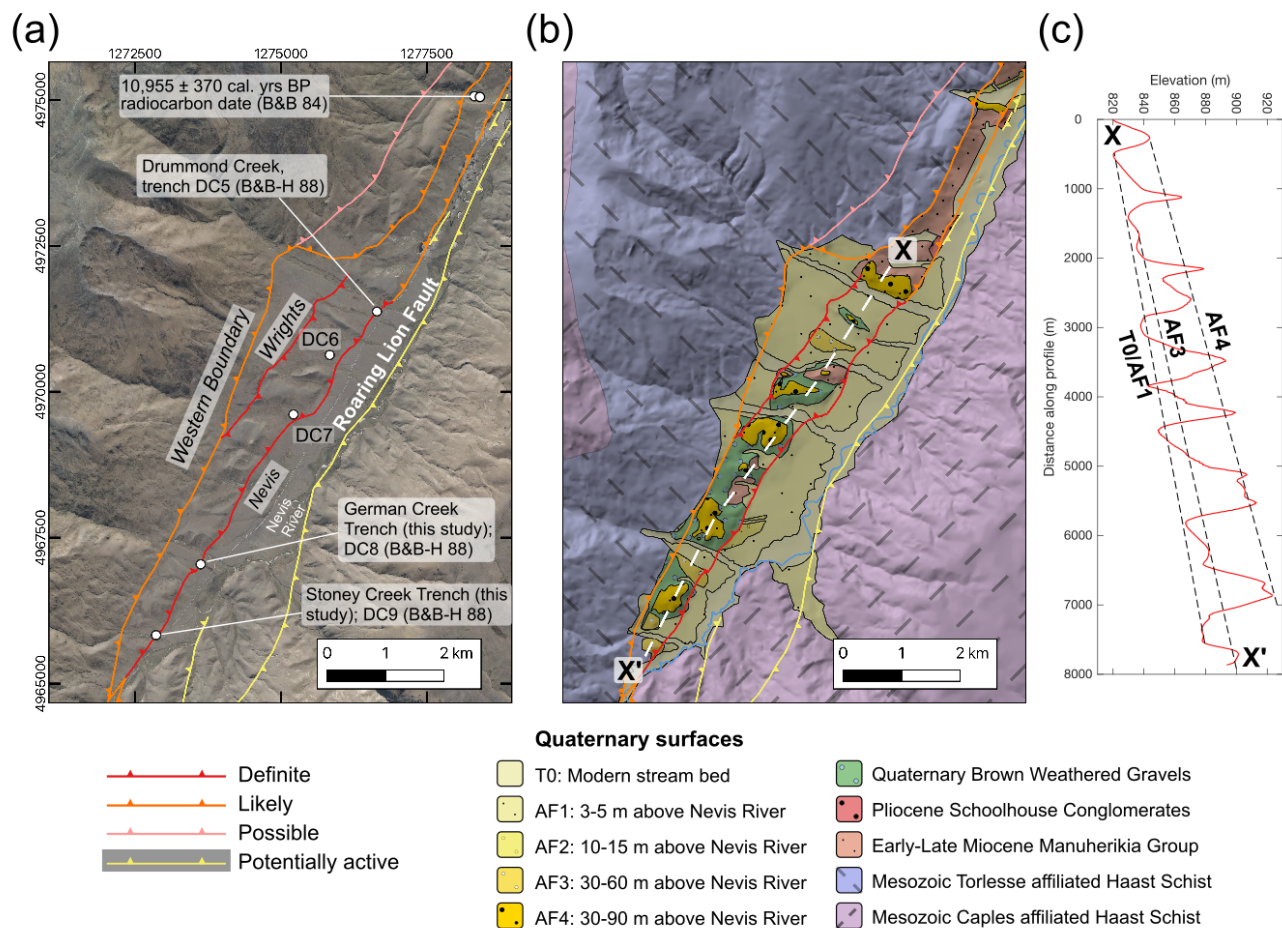


Figure 2 (a) Aerial image and (b) geologic map showing the different NCF strands (labelled in black italicised text) in the Upper Nevis valley (Beanland and Barrow, 1984a; Barrow-Hurlbert, 1985; Beanland and Barrow-Hurlbert, 1988; Turnbull, 2000; Boyce, 2002; Barrell, 2019). Trench locations from Beanland and Barrow-Hurlbert (1988) (B&B-H 88) and the location of a radiocarbon date sampled (B&B 84, Sample ID NZ 6543A; Beanland and Barrow, 1984b; Barrow-Hurlbert, 1985) from Whittens Creek is also indicated. Map extent shown in Fig. 1c, and coordinates in (a) in NZTM. (c) Topographic cross section along the Upper Nevis valley as indicated in (b) to highlight geomorphic surfaces T0 and AF1-4. Both maps underlain by the New Zealand 8 m digital elevation model.

is identified on the AF1 surface in the centre of the valley between Drummond and Stoney creeks. This strand is interpreted to be a gently dipping synthetic splay of the WBF (Beanland and Barrow-Hurlbert, 1988; Boyce, 2002). Based on progressively larger offsets of degraded AF1 surfaces at Drummond Creek, it has been proposed that the Nevis strand has accommodated at least four late Quaternary surface rupturing earthquakes (Beanland and Barrow, 1984b; Barrow-Hurlbert, 1985; Beanland and Barrow-Hurlbert, 1988). However, nowhere does the Nevis strand scarp displace T0.

Between the Nevis strand and WBF, an east dipping antithetic NCF strand extending south from Drummond Creek, termed the Wrights Fault is identified (Fig. 2a; Beanland and Barrow, 1984b; Barrow-Hurlbert, 1985; Beanland and Barrow-Hurlbert, 1988; Boyce, 2002). In combination with the Nevis strand, this has formed small structural highs in the centre of the Upper Nevis valley, across which remnants of T2-T4 are preserved (Figs. 3a and 4a). The Wrights Fault strand offsets remnants of AF3 and AF4 but does not offset the AF1 surface (Beanland and Barrow, 1984b; Barrow-Hurlbert,

1985). Hence all the most recent NCF surface ruptures in the Upper Nevis valley appear to have occurred only on the Nevis strand. There is no geomorphic evidence of lateral fault offsets in the Upper Nevis valley (Barrow-Hurlbert, 1985), or indeed elsewhere along the NCF (Barrell, 2019). Hence, we consider the NCF to be a pure dip-slip reverse fault.

3 Methods

3.1 Paleoseismic investigations and dating

Two paleoseismic trenches were excavated perpendicular to the gently-sloping ($5\text{-}10^\circ$) Nevis strand scarp on geomorphic surface AF1 in the Upper Nevis valley in March 2022 (Figs. 2, 3, and 4). The trenches, Stoney Creek (-45.385°S , 168.821°E) and German Creek (-45.374°S , 168.832°E), are close to (<100 m), but not exactly equivalent to, the bulldozer ('dozer cuts' - DC) trenches DC8 and DC9 that were previously excavated in the Upper Nevis valley (Figs 2 and S1-S4; Beanland and Barrow, 1984c; Barrow-Hurlbert, 1985; Beanland and

Barrow-Hurlbert, 1988). Our names for these trenches are taken from the informal names of creeks that run adjacent to them (Youngson et al., 2002).

The trenches were approximately 25–30 m long, 6 m wide, and 6 m deep (with a bench at 3 m depth). Trench logs were made in the field on graph paper at a 1:25 scale using a string grid. Interpretations were subsequently refined using an orthorectified mosaic of the trench wall that was generated from multiple photos of the trench walls in Agisoft Metashape (<https://www.agisoft.com/>). Due to time constraints, only the north wall of both trenches was logged.

Nine samples from the trenches were submitted for Optically Stimulated Luminescence (OSL) dating. Samples were taken using a 20 cm steel tube that was hammered into the trench walls to prevent bleaching. OSL dating was conducted at the Victoria University of Wellington Luminescence Dating Laboratory. Samples were first prepared using the fine-grained (4–11 μm) technique. Luminescence ages for the samples were then derived using the Single Aliquot Regenerative Method (SAR) to determine their Equivalent Dose (Murray and Wintle, 2000) and gamma spectroscopy to measure their Dose Rate (see Supplementary Information S3 for further details).

From combining the trench stratigraphy with the OSL dates, and their associated uncertainties, a probabilistic chronology of surface ruptures at the trench sites was constrained using Bayesian statistical modelling in OxCal v4.4.4 (Supplementary Information S4; Bronk Ramsey, 2009; Lienkaemper and Bronk Ramsey, 2009). Given the similar stratigraphy and proximity of the German Creek and Stoney Creek trenches (1.5 km apart), we developed a single OxCal model to evaluate the timing of surface ruptures at these trench sites.

Using the ‘Combine’ function in OxCal, we then evaluate the degree to which the timing of surface rupturing earthquakes in the Upper Nevis trenches can be correlated with the timings estimated elsewhere along the NCF from the Gibbston and Macdonalds Creek trenches (Fig 1b; van den Berg et al., 2023). Specifically, for each possible rupture correlation we use the Combine function to provide: (1) the chi-square statistic (χ^2) that the probability distributions functions for rupture timing are statistically distinct (at a 95% significance level), (2) an Agreement Index (A_{comb}), which is a measure of the spatial overlap between the two distributions, and (3) a combined probability distribution from summing the two rupture timing distributions (https://c14.arch.ox.ac.uk/oxcal3/arch_cmb.htm and https://c14.arch.ox.ac.uk/oxcal3/oper_an.htm#prob; Bronk Ramsey, 2009; DuRoss et al., 2011; van den Berg et al., 2023).

3.2 High resolution digital elevation models from Uncrewed Aerial Vehicle photos

We use photos taken using an Uncrewed Aerial Vehicle (UAV) and the principle of structure from motion (SfM) to generate digital surface models (DSM) at four key sites along the Nevis segment identified by Beanland and Barrow-Hurlbert (1988): Drummond Creek (Fig. 2a),

Coal Creek (Fig. 1c), and the German and Stoney creeks trench sites (Table 1).

Photos for the DSM were taken using a DJI Phantom 3 Professional UAV, which was fitted with a gimbal-stabilized 12 megapixel digital camera with a 3.6 mm focal lens. At each locality, the UAV collected photos along an automated flight plan generated for a ‘3DMapArea’ mission in the DJI GS Pro app (<https://www.dji.com/nz/downloads/products/ground-station-pro>). The photos were then processed into a DSM using Agisoft, whereby photos from the survey were first aligned and then used to build a 3D point cloud. The point cloud was then used as the source for building the DSM with the default interpolation and filtering options in Agisoft selected.

Ground control points were not used, and so the DSM’s absolute location accuracy is dependent on the UAV’s onboard global navigation satellite system (resolution 1–5 m). However, in assessing the NCF scarps, we are mainly concerned with the DSM’s internal accuracy, and these within-model errors are much lower (Kalacska et al., 2020). Unlike bare-earth digital elevation models, surface features (e.g., vegetation) are not removed from DSMs. Nevertheless, in areas with sparse vegetation, such as the Nevis valley where vegetation is dominated by ~ 0.5 m high tussocks, it has been shown that UAV-derived DSM can still resolve subtle fault scarps and offset geomorphic features (Johnson et al., 2014; Angster et al., 2016). The influence of vegetation is further reduced by using 5–50 m wide swaths to extract multiple topographic profiles across the scarp in MATLAB TopoToolbox (Schwanghart and Scherler, 2014). From the mean elevation of these profiles, we then construct regression lines through the surfaces either side of the scarp, and their vertical separation at the mid point along the scarp is taken as its vertical offset. The uncertainty in this measurement from the along-strike variations in scarp height and the offset surface’s non-planarity is quantified based on the offset of lines that represent the standard deviation of the swath’s elevation (Figs. 3c and 4c).

4 Results

4.1 Paleoseismic trench results

4.1.1 Trench wall stratigraphy

The stratigraphy of the German Creek and Stoney Creek trench walls is dominated by a light grey poorly-sorted clast-supported gravel (Unit 3, Figs. 5–7). This unit extends from the base of the trench to within 0.5 m of the surface. Clasts are pebble to boulder in size with a maximum diameter of 50 cm and are angular to sub rounded. The lithology of these clasts are predominantly schist, with a subordinate group of quartz. The upper 0.5 m of the gravel matrix grades from grey to brown, which likely reflects near surface soil development. Our description of these gravels matches those from previous trenches in the Upper Nevis valley (Beanland and Barrow, 1984c; Barrow-Hurlbert, 1985) and natural exposures of the gravel underlying the AF1 surface (Boyce, 2002).

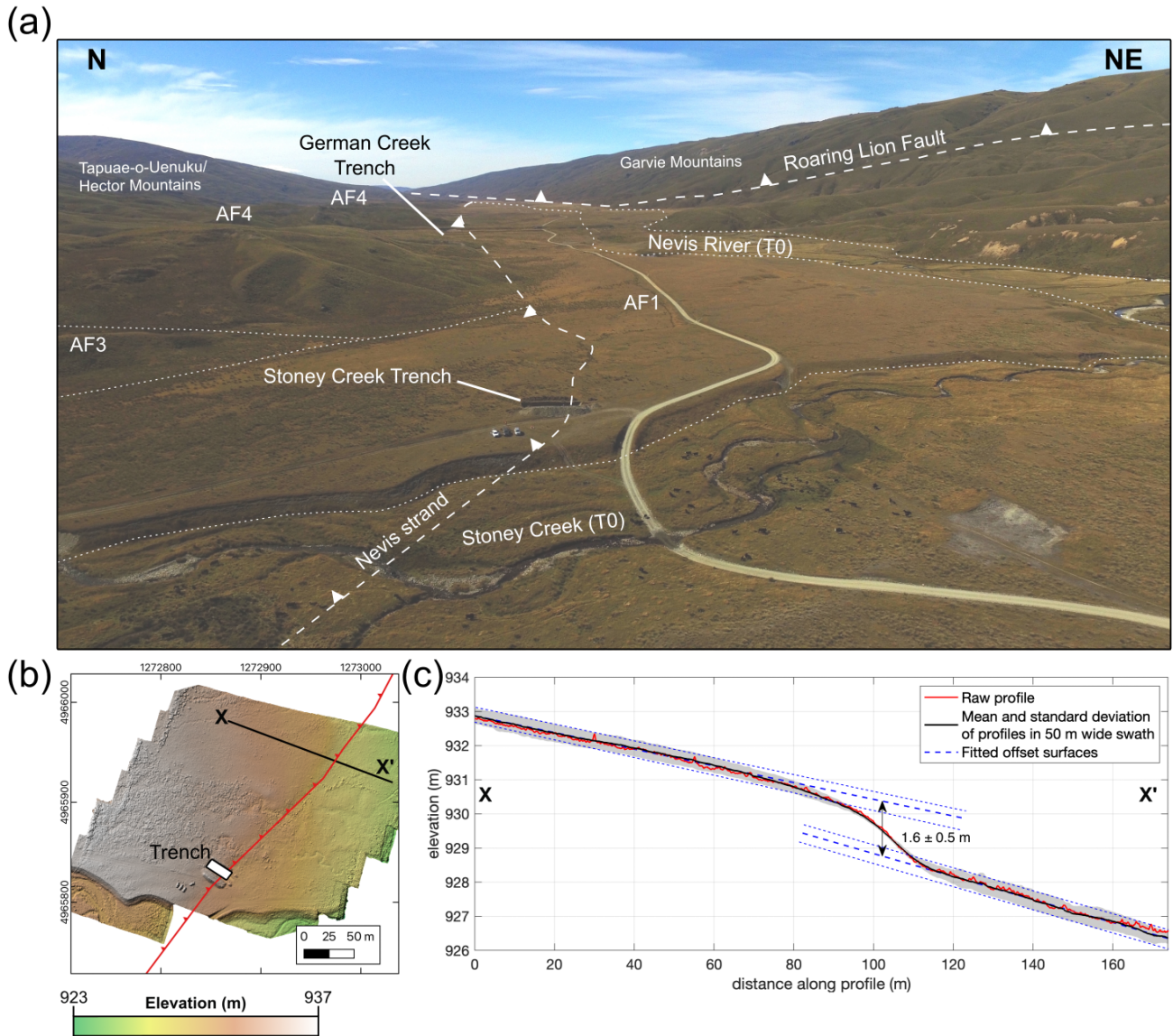


Figure 3 (a) Annotated Uncrewed Aerial Vehicle (UAV) image over the Stoney Creek trench site. Image taken looking to the north with fault traces and different geomorphic surfaces outlined. The position of the Roaring Lion Fault is based on the mapping in Turnbull (2000). (b) UAV-derived digital surface model (DSM) of the trench site. Coordinates in NZTM. (c) Vertically exaggerated topographic profile across the scarp extracted from the mean (black line) and standard deviation (grey shading) of elevation in a 50 m wide swath centered on line X-X' in (b). Dashed blue lines represent regression surfaces used to measure vertical offset across the scarp. See section 3.2 for further information on the UAV-DSM.

Site	Area (km ²)	UAV Height (m)	Number of images	Average Point Density (points/m ²)	Pixel size (cm ²)
Stoney Creek	0.063	30	176	655	16
German Creek	0.066	30	221	1122	9
Drummond Creek	0.115	50	560	232	30
Coal Creek	0.323	78	541	56.1	114

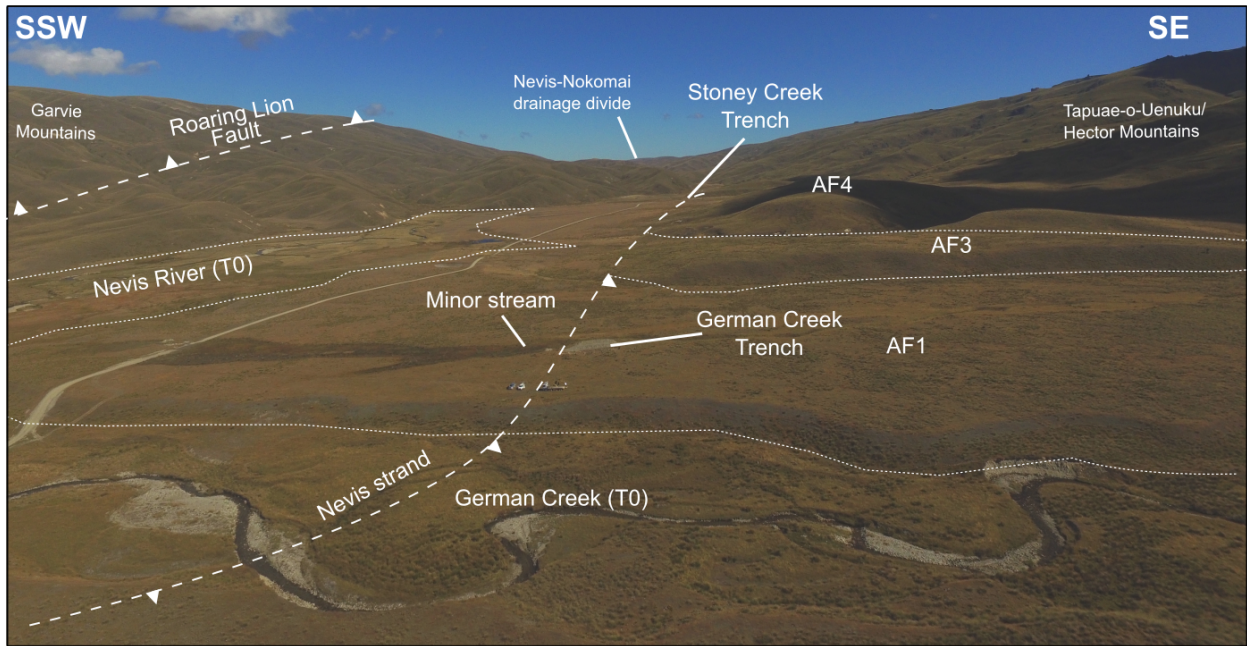
Table 1 Properties of the digital surface models (DSM) along the NCF generated from Uncrewed Aerial Vehicles (UAV) photos.

In the German Creek trench, a 5–30 cm thick bed of matrix-poor pea-gravels with well sorted sub-rounded pebbles is encountered near the top of Unit 3 (Figs. 6 and 7). We mapped this bed as a facies within Unit 3 (Unit 3a). It comprises two fining upward sequences in which pebbles grade up from 5 to 0.5 cm diameter. Unit

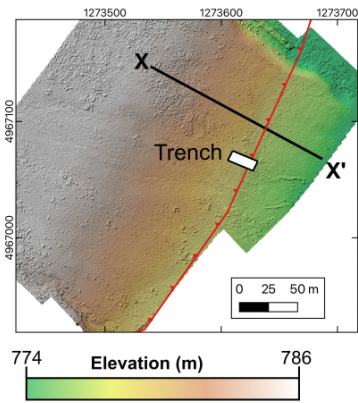
3a cannot be identified within the main zone of trench deformation (Fig. 6). We infer this is because of sediment mixing during faulting and folding.

Near the foot of the scarp in both trenches is a distinct gravel (Unit 2) that is distinguished from Unit 3 by being matrix-supported and containing fewer cobbles (maxi-

(a)



(b)



(c)

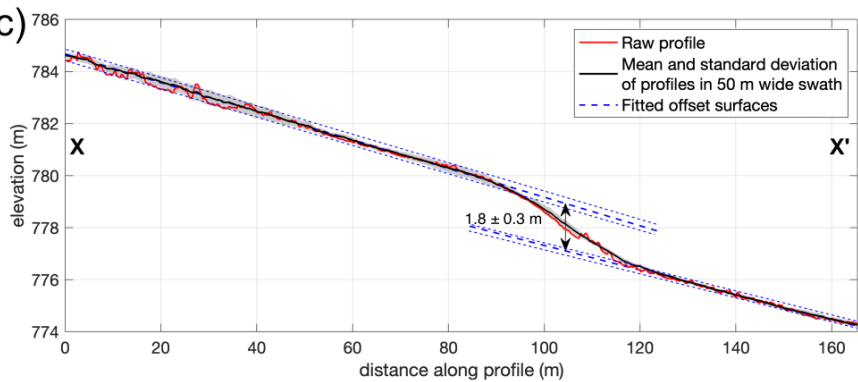


Figure 4 UAV image looking south over the German Creek trench site. (b) DSM of the trench site, coordinates in NZTM. (c) Topographic profile across the scarp, with vertical separation across the scarp measured using the mean and standard deviation of profile lines in a 50 m wide swath around line X-X' in (b).

num clast size 15 cm, Figs. 5-8). Overlying Units 2 and 3 is a medium brown, massive very-well sorted silt (Unit 1) that we interpret as a loess deposit, and a brown-grey friable medium-grained soil that contains rootlets (Unit 0).

4.1.2 Deformation history

We identified four gently-dipping ($<30^\circ$) synthetic faults in each trench from offset unit contacts and clast alignment along their trace. In addition, we traced faults from shallow cracks in the trench wall. We infer these cracks are a consequence of gravel-on-gravel displacements and later downward groundwater percolation, which made the faults relatively erodible during trench excavation. Three of the Stoney Creek trench faults terminate within the structureless Unit 3 gravels and so it is not possible to measure the offset across them (Fig. 5). Fault F4 has folded and thickened the Unit 2 gravels (Fig. 8b). However, this unit has limited lateral extent, and as a possible slope or colluvial deposit (see

discussion below) its base was not necessarily a planar horizontal surface. We therefore do not consider that its offset across F4 is a reliable offset marker. Consequently the offset across individual faults in the Stoney Creek trench, and the degree to which deformation has been accommodated by faulting or folding at this site, is unknown.

Using the top of Unit 3a in the German Creek trench as an offset marker, which can be correlated either side of the four faults, the total throw accommodated by the faults in this trench is ≤ 1.0 m (Fig. 6). Given the 1.8 m vertical separation of the AF1 surface at German Creek (Fig. 4c), we infer the remaining deformation is accommodated by folding.

We interpret that the Upper Nevis valley trenches provide stratigraphic evidence for two surface rupturing earthquakes. In the penultimate rupture, a combination of folding and rupture along the synthetic low angle trench faults formed a gently dipping scarp, as is typical for low angle thrust faults ($<30^\circ$ dips) like the Nevis

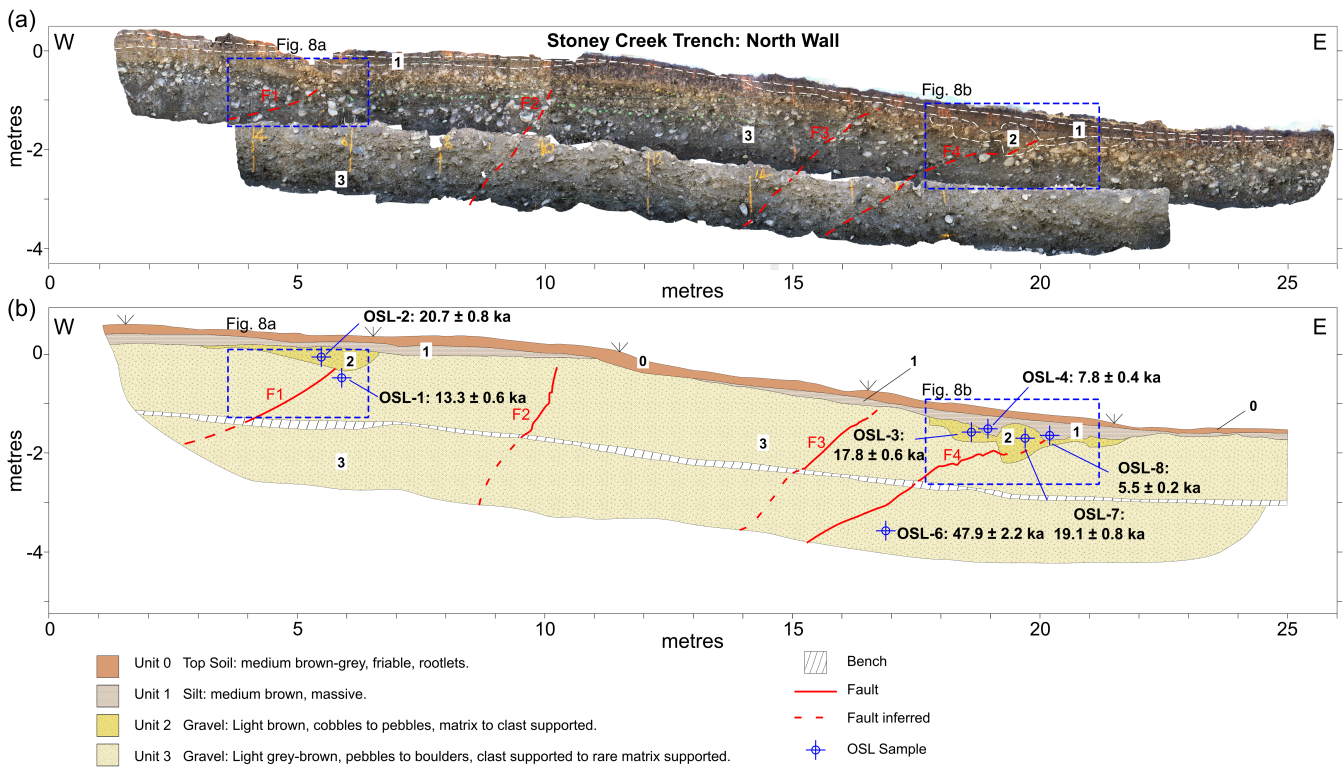


Figure 5 (a) Orthorectified mosaic and (b) trench log for the upper and lower walls of the Stoney Creek trench, (north wall). Please note, (a) consists of separate orthomosaics for the upper and lower trench walls, and which has resulted in some image overlap around the bench. An unannotated version of the orthomosaic in (a) is available at: <https://zenodo.org/doi/10.5281/zenodo.10819579>.

strand (McCalpin and Carver, 2009). This deformation style is in contrast to other NCF trenches where displacement was localised on a single fault strand; however in these cases, the trenches were excavated across moderate-steeply dipping (45–66°) antithetic (Macdonalds Creek) or master (Gibbston) NCF strands (Beanland and Barrow-Hurlbert, 1988; van den Berg et al., 2023).

We then infer that the scarp was subject to gravity and/or slope wash processes that reworked the Unit 3 gravels adjacent to the scarp into distinct matrix-supported Unit 2 gravels (Fig. 8). A distinct ~1 m wide lens of gravels within Unit 3 in the Stoney Creek trench may also represent reworked gravels that formed above Fault F1 (Figs. 5 and 8a). Unit 2 was then deformed by the most recent surface rupture as evidenced from the folding and thickening of the Unit 2 gravels around fault F4 in the Stoney Creek trench, and faults F3 and F2 in the German Creek trench (Fig. 8). This was followed by deposition of Unit 1 loess, which is locally thickened in the depressions created by Unit 2 folding.

4.1.3 OSL dating results and surface rupture timing

We estimate the timing of the two surface rupturing earthquakes we inferred from the Upper Nevis valley trench stratigraphy by incorporating the OSL dates presented in Table 2 into a probabilistic rupture chronology using OxCal (Fig. 9, Supplementary Information S4). Two OSL dates were returned from Unit 3 gravels: OSL-1 (13.3 ± 0.6 ka) and OSL-6 (47.9 ± 2.2 ka). However,

as OSL-1 is not in stratigraphic order with the overlying dates (Fig. 5), we suggest its luminescence signal has been partially reset. We therefore do not consider this date further.

OSL dates OSL-2 (20.7 ± 0.8 ka), OSL-3 (17.8 ± 0.6 ka), OSL-7 (19.1 ± 0.8 ka), and OSL-10 (11.9 ± 0.6 ka) were all sampled from Unit 2 (Table 2). Given that Unit 2 is relatively thin (0.5 m), and the consistency between this unit’s other OSL dates, we regard OSL-10 as an outlier that we exclude from our OxCal model. The remaining dates for Unit 2 are grouped as a single *phase* in OxCal (Fig. 9). The OSL dates from Unit 1 loess are 7.8 ± 0.4 ka (OSL-4), 5.5 ± 0.2 ka (OSL-8), and 4.3 ± 0.2 ka (OSL-9, Table 2).

The stratigraphic evidence for the penultimate surface rupturing earthquake (UN-eq2) is provided by the Unit 2 gravels at the foot of the scarp. One approach to date this rupture would be to formally interpret these gravels as a colluvial wedge, and hence the Unit 2 OSL-dates are a very close minimum age estimate for this event. This interpretation implies that the Nevis scarp has been significantly eroded, as its current slope angle (5-10°) is below the angles normally assumed for colluvial deposits to accumulate (>20°; Carretier et al., 2002; McCalpin and Carver, 2009; Chiama et al., 2023). An alternative -but not mutually exclusive- interpretation is that the Nevis strand scarp represents a pressure ridge scarp, which are generally not associated with significant colluvial deposits, but are subject to slope wash processes (McCalpin and Carver, 2009). We ten-

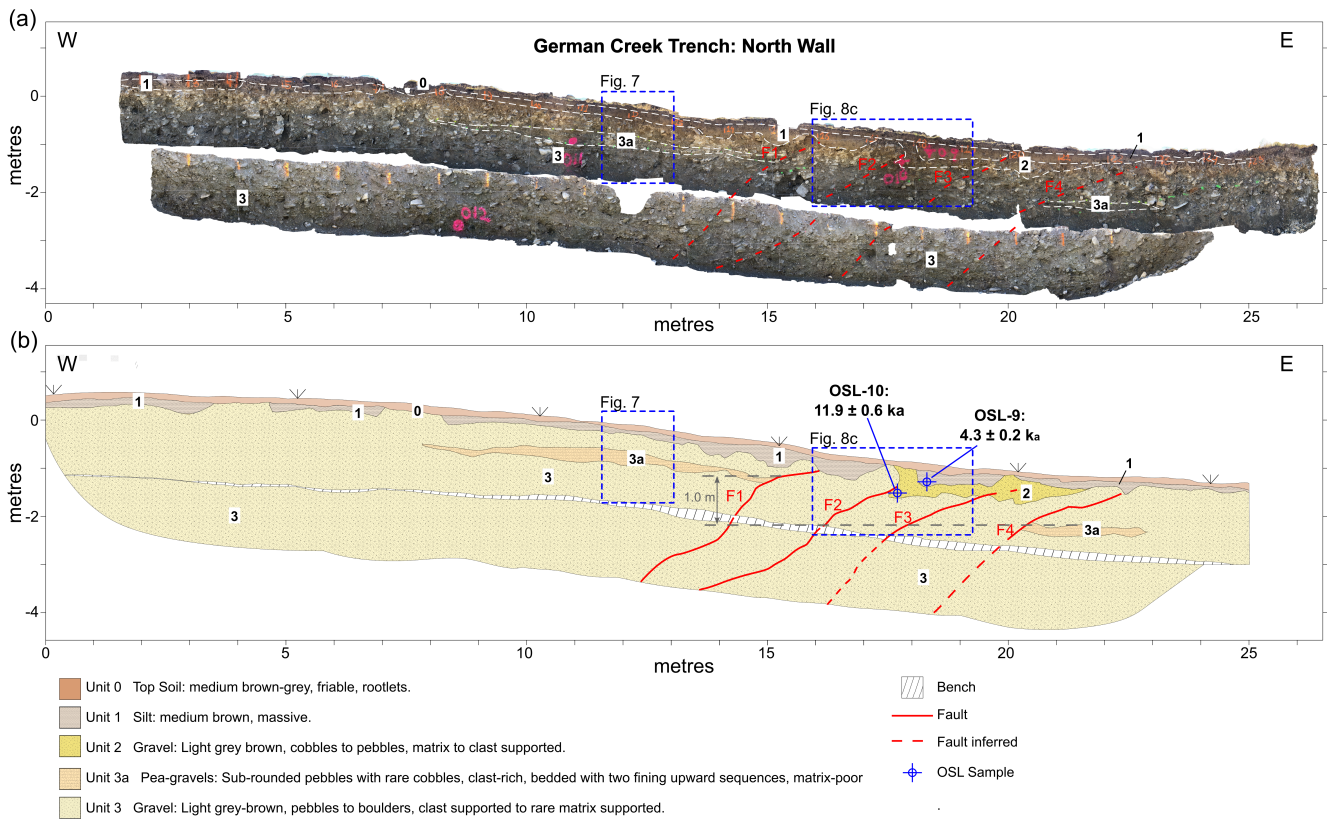


Figure 6 (a) Orthorectified mosaic and (b) trench log for the upper and lower walls of the German Creek trench (north wall). As with Fig. 5, (a) consists of two separate orthomosaics, one for each trench wall, and this has resulted in some overlap between them. The vertical separation of the top of Unit 3a between faults F1-F4 is also indicated. An unannotated version of the trench wall orthomosaic is available at <https://zenodo.org/doi/10.5281/zenodo.10819579>.

tatively prefer the latter interpretation as Unit 2's ~ 18-20 ka age indicates that UN-eq2 occurred during the last glacial period when the Nevis Valley was experiencing a periglacial climate (Barrow-Hurlbert, 1985), and frequent freeze-thaw cycles would have promoted solifluction and debris flow processes around the scarp to form Unit 2 (Font et al., 2006; McCalpin and Carver, 2009). In either case, UN-eq2's timing is most appropriately constrained by date OSL-6 (Unit 3, 47.9 ± 2.2 ka) and the grouped dates from Unit 2, albeit with the recognition that Unit 2 dates likely providing a close minimum estimate given that OSL-6 was sampled near the base of the trench. To recognise this, we use the *Zero Boundary* command in OxCal to negatively skew UN-eq2's timing probability distribution function (DuRoss et al., 2011). This leads to a 28.9^{+12.9}_{-9.1} ka (95% uncertainty) estimate for UN-eq2's timing (Fig. 9).

The most recent surface rupture (UN-eq1) is represented by folding and reverse fault offsets in Unit 2, with Unit 1 deposited after this rupture. From combining the OSL dates from Units 1 and 2 into our OxCal model, the timing of UN-eq1 is estimated to be 12.7 ± 4.9 ka (Fig. 9). We discuss the OSL dates and estimated rupture timing further in Section 5.1.

4.1.4 Integration of paleoseismic data along the NCF

Following the steps outlined in Section 3.1, the surface rupture timings inferred from the Upper Nevis valley

trenches are correlated with timings from elsewhere along the NCF at Gibbston and Macdonalds Creek (Table 3 and Fig. 10). We note that a 3-event interpretation was originally proposed for the Gibbston trench (Beanland and Barrow-Hurlbert, 1988), however, we consider a revised 2-event interpretation here only (van den Berg et al., 2023). For each correlation, we assign a score between 1-3 where: 1 means the events cannot be correlated as the comparisons fail the χ^2 test at a 95% significance level or there is a zero distribution (i.e., no overlap in the respective rupture timing distribution functions), 2 indicates that correlation passes the χ^2 test, however, the agreement indices (A_{comb}) for the combined or individual ages are below the recommended level of 60% (Bronk Ramsey, 2009; DuRoss et al., 2011), and 3 indicates no statistical reason why the ruptures cannot be correlated.

This comparison indicates that we cannot exclude the possibility that rupture UN-eq1 correlates with the most recent surface rupture inferred from the Gibbston Trench (G-eq1), or with G-eq1 and the most recent surface rupture recorded at the Macdonalds Creek trench (MC-eq1, Table 3). However, the correlation is weak in these cases, with the individual agreement index for G-eq1's timing below the recommended threshold (60%). UN-eq1 can also be correlated with the penultimate ruptures inferred from the Gibbston (G-eq2) and Macdonalds Creek trenches (MC-eq2). If true, this would imply that events G-eq1 and MC-eq1 did not extend to the Up-

Laboratory Code	Field Code	Trench ¹	Unit	Water Content (%)	U (ppm) from ²³⁴ Th	U (ppm) from ²²⁶ Ra, ²¹⁴ Pb, ²¹⁴ Bi	U (ppm) from ²¹⁰ Pb	Th (ppm) from ²⁰⁸ Tl, ²¹² Pb, ²²⁸ Ac	K (%)	Equivalent Dose (Gy)	Cosmic Dose Rate (Gy/kyr)	Dose Rate (Gy/kyr)	OSL Age (ka)	Modelled Age (ka)
WLL1544	OSL-1	SC	3	25.4	2.81±0.27	2.62±0.14	2.61±0.21	11.21±0.13	1.50±0.03	43.37±1.10	0.2178±0.0109	3.27±0.11	13.3±0.6	N/A ²
WLL1545	OSL-2	SC	2	14.7	1.80±0.18	1.45±0.09	1.71±0.15	6.07±0.08	1.03±0.02	50.38±1.35	0.2402±0.0120	2.43±0.06	20.7±0.8	20.6 ±1.6
WLL1546	OSL-3	SC	2	20.6	2.37±0.22	1.86±0.10	1.98±0.16	7.77±0.09	1.35±0.03	49.90±0.89	0.2303±0.0115	2.80±0.09	17.8±0.6	17.8 ±1.2
WLL1547	OSL-4	SC	1	28.1	2.31±0.23	2.07±0.12	2.05±0.18	7.90±0.10	1.01±0.02	19.07±0.52	0.2271±0.0114	2.44±0.09	7.8±0.4	7.7±0.8
WLL1549	OSL-6	SC	3	9.5	1.61±0.17	1.53±0.09	1.35±0.13	6.11±0.08	1.53±0.03	135.45±5.67	0.1602±0.0080	2.83±0.05	47.9±2.2	48.2±4.4
WLL1550	OSL-7	SC	2	29.3	2.01±0.20	1.60±0.10	1.69±0.15	6.08±0.08	0.83±0.02	37.19±0.8	0.2303±0.115	1.95±0.07	19.1±0.8	19.0±1.6
WLL1551	OSL-8	SC	1	16.7	2.72±0.28	2.28±0.15	1.96±0.20	7.74±0.11	0.97±0.02	14.94±0.51	0.2303±0.115	2.73±0.07	5.5±0.2	5.4±0.4
WLL1552	OSL-9	GC	1	28.1	3.52±0.31	2.84±0.15	2.92±0.22	10.87±0.13	1.11±0.02	13.55±0.28	0.2402±0.012	3.71±0.12	4.3±0.2	4.2±0.4
WLL1553	OSL-10	GC	2	35.0	2.85±0.27	2.26±0.13	2.59±0.21	9.46±0.12	1.43±0.03	34.44±0.96	0.2368±0.118	2.90±0.13	11.9±0.6	N/A ²

Table 2 Optically Stimulated Luminescence (OSL) data and ages from the Upper Nevis valley trenches. K = potassium; U = uranium; Th = thorium; Ra = radon; Tl = thallium; Pb = lead; Bi = bismuth; Ac = actinium; Gy = Grays; ky = 1000 years before present (BP). OSL age uncertainty reported at 1 standard deviation (σ). ‘Modelled age’ are those derived from the OxCal model (Fig. 9, Supplementary Information S4), and the reported uncertainties are $\pm 2\sigma$.

¹SC: Stoney Creek, GC: German Creek

²OSL date not included in OxCal model

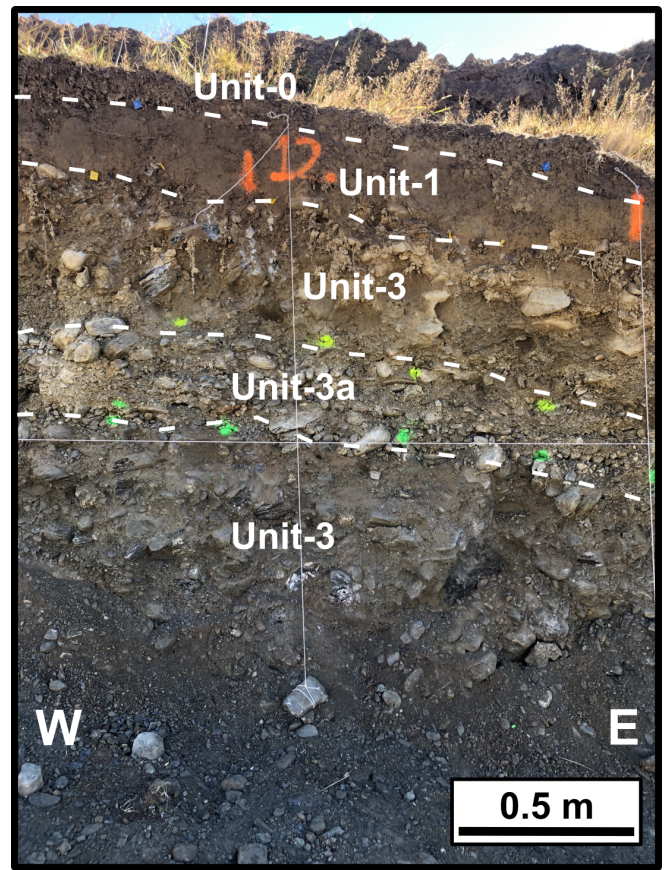


Figure 7 Cross section of the trench wall stratigraphy away from the scarp in the German Creek trench (north wall) highlighting the Unit 3a pea gravel facies. Location of image within trench indicated in Fig. 6.

per Nevis valley. Alternatively, the penultimate surface rupture in the Upper Nevis valley (UN-eq2) could be correlated with G-eq2 and MC-eq2 (Table 3).

As with any integration of surface rupture timings between paleoseismic trenches, it is also possible that the ruptures inferred from the NCF trenches are independent, or distinct but temporally clustered, events. In particular, since incremental fault displacements in the NCF trenches are bracketed by the relative offset of different stratigraphic layers (Figs. 5-8; Beanland and Barrow-Hurlbert, 1988; van den Berg et al., 2023), there are relatively high timing uncertainties, which in turn makes it challenging to exclude rupture correlations. We discuss this further in Section 5.2.

4.2 Re-examination of late Quaternary NCF activity using high resolution digital surface models

4.2.1 Drummond Creek

Beanland and Barrow-Hurlbert (1988) identified five small but distinct geomorphic surfaces just south of Drummond Creek (Fig. 2a), which they interpreted as a flight of degradation surfaces that formed during short periods of stability as the AF1 surface was progressively eroded. Using topographic profiles constructed from theodolite measurements with 500 mm accuracy, they also identified a correlation between the relative age of

Rupture Correlation	χ^2 Statistic	p	A_{comb} (%)	Correlation Score
UN-eq1 - G-eq1	1.712	>0.05	62.8	2 ³
UN-eq1 - G-eq2	1.436	>0.05	66.8	2 ⁴
UN-eq1 - G-eq1 - MC-eq1	1.846	>0.05	72.7	2 ³
UN-eq1 - G-eq2 - MC-eq1	4.343	>0.05	39.9	2
UN-eq1 - G-eq1 - MC-eq2	12.49	<0.05	6.1	1
UN-eq1 - G-eq2 - MC-eq2	1.689	>0.05	76.8	3
UN-eq2 - G-eq1	13.468	<0.05	1.6	1
UN-eq2 - G-eq2	0.094	>0.05	138.6	3
UN-eq2 - G-eq2 - MC-eq1	14.267	<0.05	2.6	1
UN-eq2 - G-eq2 - MC-eq1	17.748	<0.05	1.2	1
UN-eq2 - G-eq1 - MC-eq2	26.034	<0.05	0.2	1
UN-eq2 - G-eq2 - MC-eq2	0.328	>0.05	141	3

Table 3 Results of rupture timing correlation tests between trenches along the NCF. UN: Upper Nevis trenches, G: Gibbston trench, MC: Macdonalds Creek trench (van den Berg et al., 2023). In this analysis, we apply a revised interpretation of the original Gibbston trench study (Beanland and Barrow-Hurlbert, 1988), which is presented in van den Berg et al. (2023).

³Individual A_{comb} for G-eq1 < 60%

⁴Individual A_{comb} for G-eq2 < 60%

these surfaces and their vertical separation across the Nevis strand scarp. In turn, this was used to suggest that four surface rupturing earthquakes, each with 0.25–0.4 m vertical displacement, had occurred at this site since AF1 abandonment (Beanland and Barrow, 1984b; Barrow-Hurlbert, 1985; Beanland and Barrow-Hurlbert, 1988). This represents a significant difference from our interpretation of two surface ruptures recorded at the German and Stoney creek trenches, and which were excavated across the same AF1 surface 5 km south of Drummond Creek (Section 4.1.2).

To investigate this discrepancy, in Fig. 11 we show revised measurements for the geomorphic surface's vertical separation across the Nevis strand scarp at Drummond Creek, which we measured using a UAV-derived DSM (Section 3.2). This indicates that vertical separation across the undegraded AF1 surface (1–1.3 m, profiles A-A' and C-C', Fig 11c) is distinctly higher than the degraded surfaces (0.4–0.7 m). However, unlike the theodolite topographic profiles, we find that the vertical separation across the highest degraded AF1 surface (0.7 m, Profile D-D', Fig. 11c) is comparable to the vertical separation across the scarp on the middle (0.4 m, Profile B-B') and lowest (0.7 m, Profile E-E') degraded surfaces. Furthermore, a profile across the these surfaces (Profile F-F') indicates that the lowest and middle degraded surfaces mapped by Beanland and Barrow-Hurlbert (1988) may be equivalent surfaces (Fig. 11c). We also do not observe the highest degraded AF1 surface in the scarp's footwall (Fig. 11b). This suggests that erosion to form this surface was limited to the upthrown side of the scarp.

It is possible that the variations in vertical offset across the different surfaces at Drummond Creek represents the along-strike variability of displacement in a single rupture. However, our preferred interpretation is that the differences in offset between the undegraded (1–1.3 m) and degraded (0.4–0.7 m) surfaces represent progressive offset of two surface ruptures since AF1 abandonment. Importantly, and unlike Beanland and Barrow-Hurlbert (1988), we do not find a correlation between the degraded surface's relative age and their vertical offset (Fig. 11c), and so it is unlikely that the

number of ruptures recorded at Drummond Creek since AF1 abandonment is >2.

In summary, we suggest the following sequence of events at Drummond Creek following AF1 abandonment: (1) surface rupture and offset of the undegraded AF1 surface, (2) progressive erosion of the AF1 surface, (3) a subsequent surface rupture that offset both AF1 and its degraded surfaces, and (4) continued downcutting by Drummond Creek to its current unfaulted floodplain (T0). This sequence of events is therefore consistent with the number and timing of events inferred from German and Stoney Creek trenches (assuming that the penultimate event inferred from the trenches occurred after AF1 abandonment), and with the progressive offsets at the DC7 trench locality (Fig. 2a), where the AF1 surface and a single degraded AF1 surface are vertically offset by 1.4 m and 0.6 m respectively (Beanland and Barrow, 1984b; Barrow-Hurlbert, 1985).

4.2.2 Coal Creek

Multiple NCF strands are identified in the Lower Nevis valley (Fig. 12a; Williams, 1974; Beanland et al., 1984; Beanland and Barrow-Hurlbert, 1988; Turnbull, 2000; Barrell, 2019). This 13 km long structurally-controlled basin is akin to the Upper Nevis valley, with the NCF's main strand ('Schoolhouse Strand') juxtaposing Torlesse terrane affiliated Haast Schist over a sequence of late Cenozoic sediments on its western side and the Roaring Lion Fault bounding the valley to the east (Beanland et al., 1986; Turnbull, 2000; Barrell, 2019). During their investigations Beanland and Barrow-Hurlbert (1988) identified a ~1 km long NE trending uphill-facing scarp just north of Coal Creek. The vertical separation across the scarp was reported as 2 m on an alluvial surface immediately above the flood plain of an unnamed Coal Creek tributary, and 1 m on the flood plain itself. This scarp does, however, exhibit some enigmatic features: (1) it cannot be identified on higher terraces along-trend south of Coal Creek, and (2) it lies 4 km across-strike from the nearest NCF scarp, which is unusually high compared to elsewhere along the NCF and to other reverse faults in the Otago range and basin reverse fault province (Fig. 12a; Van Dissen et al., 2007;

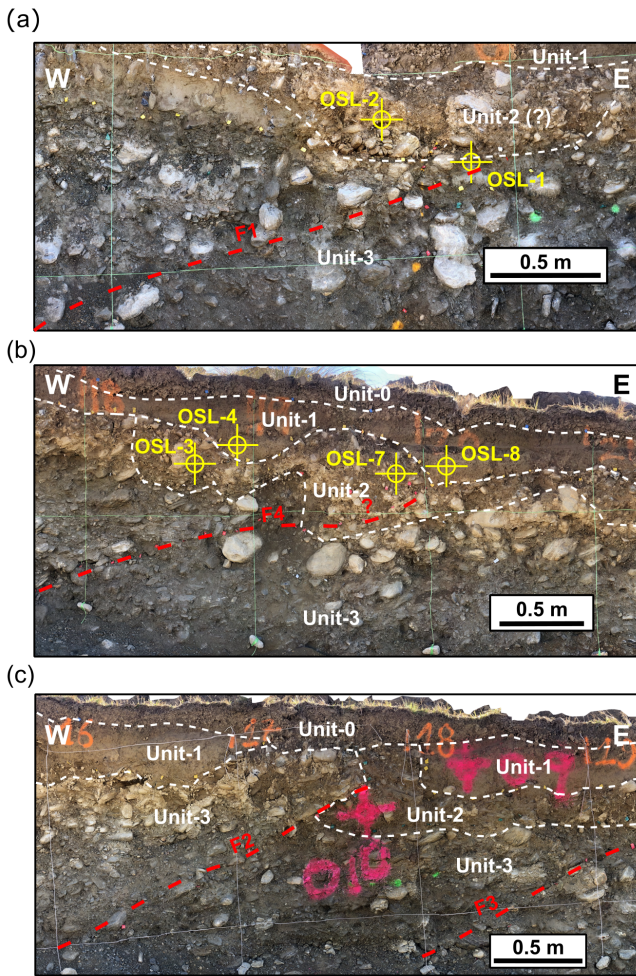


Figure 8 Examples of fault deformation identified from the trench walls. (a) Termination of fault F1 at the Unit 2-3 contact in the Stoney Creek trench north wall. Folding and thrusting of Units 2 and 3 during the most recent surface rupture in (b) Stoney Creek and (c) German Creek trenches. In (b) it is unclear whether Fault F4 extends into and offset Unit 2 during the most recent surface rupture, or if Fault F4 terminates within Unit 3 gravels but did subsequently fold and thicken the overlying Unit 2 during the most recent event. Position of images within the trench log are shown in Figs. 5 and 6.

Barrell, 2019; van den Berg et al., 2023; Griffin et al., 2022a).

The feature identified as a scarp is visible in the DSM (Fig. 12b). However, in detail it does not truly offset the Coal Creek alluvial surface (Profiles B-B' and C-C', Fig. 12c); instead there is a back limb to the northwest so that it forms a NNE trending ridge that can be traced northwards to an unnamed Coal Creek tributary. This ridge forms a 0.5 m high step in the tributary's flood plain (Profile A-A', Fig. 12c). However, the significance of this step is unclear as there is a slight convex down shape to the overall topographic profile.

Cumulatively, we suggest that there is limited evidence that the geomorphic surfaces north of Coal Creek are separated by a NCF scarp. Furthermore, this feature could alternatively represent a NNE-SSW trending strike ridge within the underlying Miocene strata (Dun-

stan Formation quartz sand to Bannockburn Formation oil shales; Turnbull, 2000)). This latter interpretation is consistent with steeply dipping N-S striking late Cenozoic strata mapped elsewhere in the Lower Nevis valley (Williams, 1974; Turnbull, 2000) and accounts for why this feature could not be mapped on higher terraces south of Coal Creek. If true, then evidence for late Quaternary NCF surface rupturing earthquakes in the Lower Nevis valley are limited to the Ben Nevis and Curving scarps (Fig. 12a; Beanland et al., 1984; Beanland and Barrow-Hurlbert, 1988). These scarps are found only on mid- high-level terraces in the Lower Nevis valley, and there are no scarps on Schoolhouse Flat, a significant outwash fan that lies adjacent to the Ben Nevis scarp (Fig. 12a).

5 Discussion

5.1 NCF activity in the Upper Nevis valley

The OSL dates returned from the Stoney Creek and German Creek trenches provide some of the first chronostratigraphic constraints for the faulted alluvial fan sequence in the Upper Nevis valley. Previously, this was limited to a radiocarbon date from Whittens Creek, which indicated a maximum age for the unfaulted floodplain (T0) of $10,955 \pm 370$ cal. years BP (Fig. 2; Beanland and Barrow, 1984b; Barrow-Hurlbert, 1985). This is consistent with our estimate for the timing of the most recent rupture in the Upper Nevis trenches (UN-eq1: 12.7 ± 4.9 ka). However, compared to our documentation of four faults within the German and Stoney Creek trench walls and evidence for two events, only a single fault and no evidence for incremental displacements was identified within the equivalent trenches from the 1980's (Figs. S1-S4; Beanland and Barrow, 1984c; Barrow-Hurlbert, 1985; Beanland and Barrow-Hurlbert, 1988). This discrepancy may result from the subtle fault expressions and changes in lithology near the top of the trenches that were key to our trench interpretation (Fig. 8), and that were not well preserved in the 1980's trenches (Fig. S4). In turn, this likely reflects that the 1980's trenches were excavated using a bulldozer and at a time when best practice for cleaning and logging trenches in Aotearoa New Zealand was still being established. The different trench interpretations may also reflect real ~ 100 m scale along-strike variations in the Nevis strand's expression; indeed, there are examples of trenches across South Island reverse faults where the opposing trench walls a few metres apart do not necessarily match one another (Barrell et al., 2020; Griffin et al., 2022a; van den Berg et al., 2023). This comparison highlights how caution should be applied when using interpretations from paleoseismic trenches to inform seismic hazard assessment, as these interpretations are not always reproducible and may change as the science evolves.

Obtaining representative slip rate estimates for the NCF's Nevis segment is challenging as the trench data only provides constraints over 1–2 recurrence intervals, one of which is still open. Hence, these data are not necessarily representative of the Nevis segment's long-term

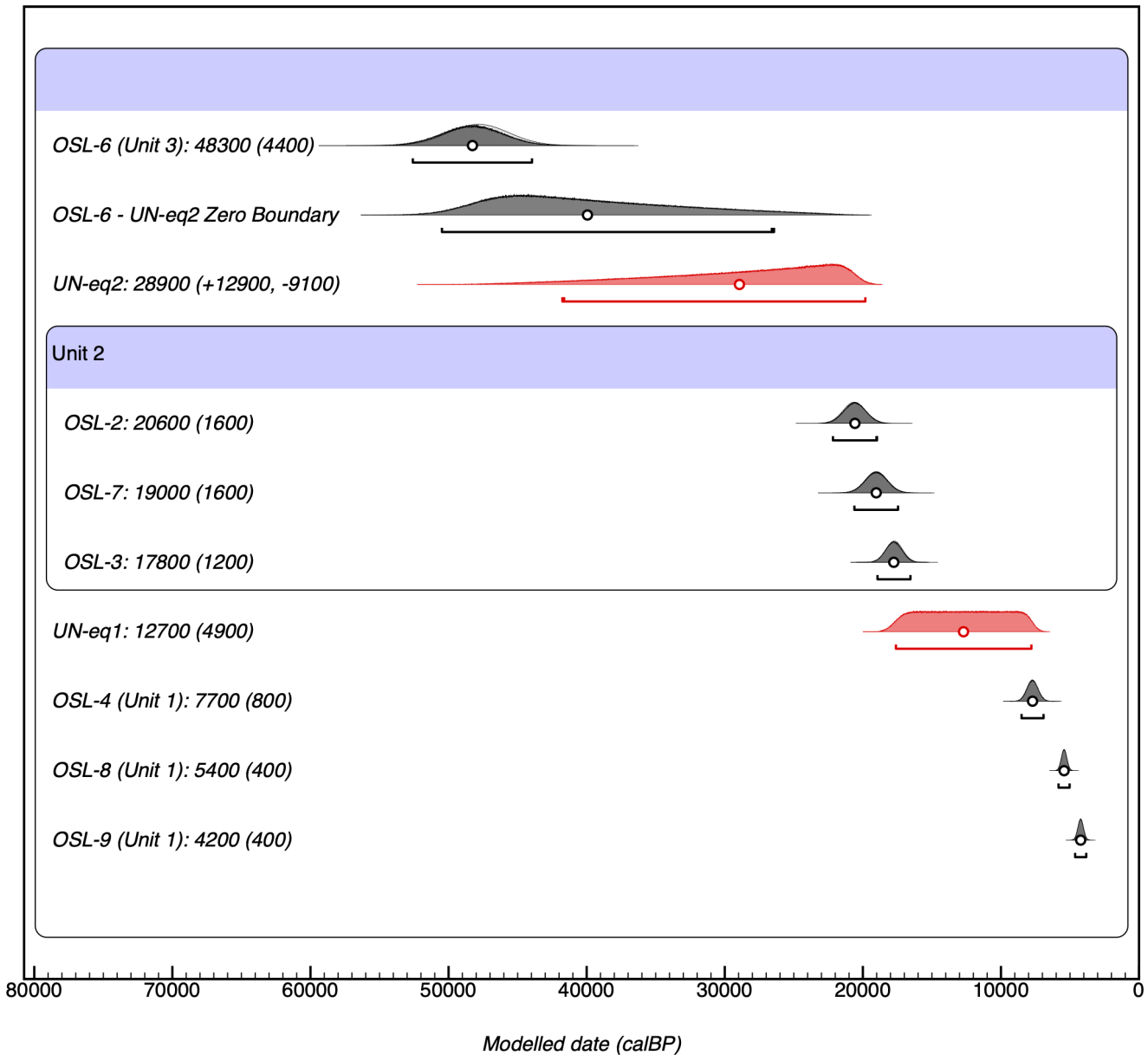


Figure 9 OxCal model for the combined chronology of the Stoney Creek and German Creek trenches including posterior distributions for the timings of the penultimate (UN-eq2) and most recent surface ruptures (UN-eq1). Light and dark grey shading indicates probability distributions for the original and posterior distributions of the OSL ages, respectively. Numbers reported by labels, and the white circles and horizontal bars in the plots, represent the mean and 95.4% uncertainty of the posterior distributions.

slip rate (Styron, 2019). To account for this, in Table 4 we compile a range of short and long-term NCF slip rate constraints. These constraints first consider that from combining the range of throw estimates across the Nevis strand scarp at Stoney, German, and Drummond creeks on the AF1 surface (1.4 ± 0.4 m) with the single OSL date from Unit 3 (OSL-6: 47.9 ± 2.2 ka), we obtain an uplift rate estimate of 0.03 ± 0.01 mm/yr ('AF1 surface-1', Table 4). Then from assuming a nominal range of fault dip estimates for the Nevis segment ($45^\circ \pm 15^\circ$; Seebeck et al., 2024), we can estimate a $0.04^{+0.03}_{-0.015}$ mm/yr slip rate.

It is possible that the layer from which OSL-6 was sampled has a greater vertical offset than the scarp but

the evidence for progressive offset during AF1 aggradation could not be recognised within the structureless Unit 3 gravels. Hence, this slip rate estimate is a minimum constraint (Table 4). A maximum constraint can be derived by combining the OSL-6 date with observations from trenches DC5-DC7 in the Upper Nevis valley (Fig. 2b), where the base of Unit 3 gravels was exposed and is vertically offset by 2.6 ± 0.9 m (Barrow-Hurlbert, 1985). This results in an uplift and slip rate of 0.05 ± 0.02 mm/yr and $0.08^{+0.07}_{-0.04}$ mm/yr respectively ('Base of Unit 3 gravels', Table 4). Alternatively, from our interpretation that the Unit 2 gravels postdate the penultimate Nevis strand surface rupture, and combining this unit's oldest date (OSL-2: 20.7 ± 0.8 ka) with the AF1 scarp off-

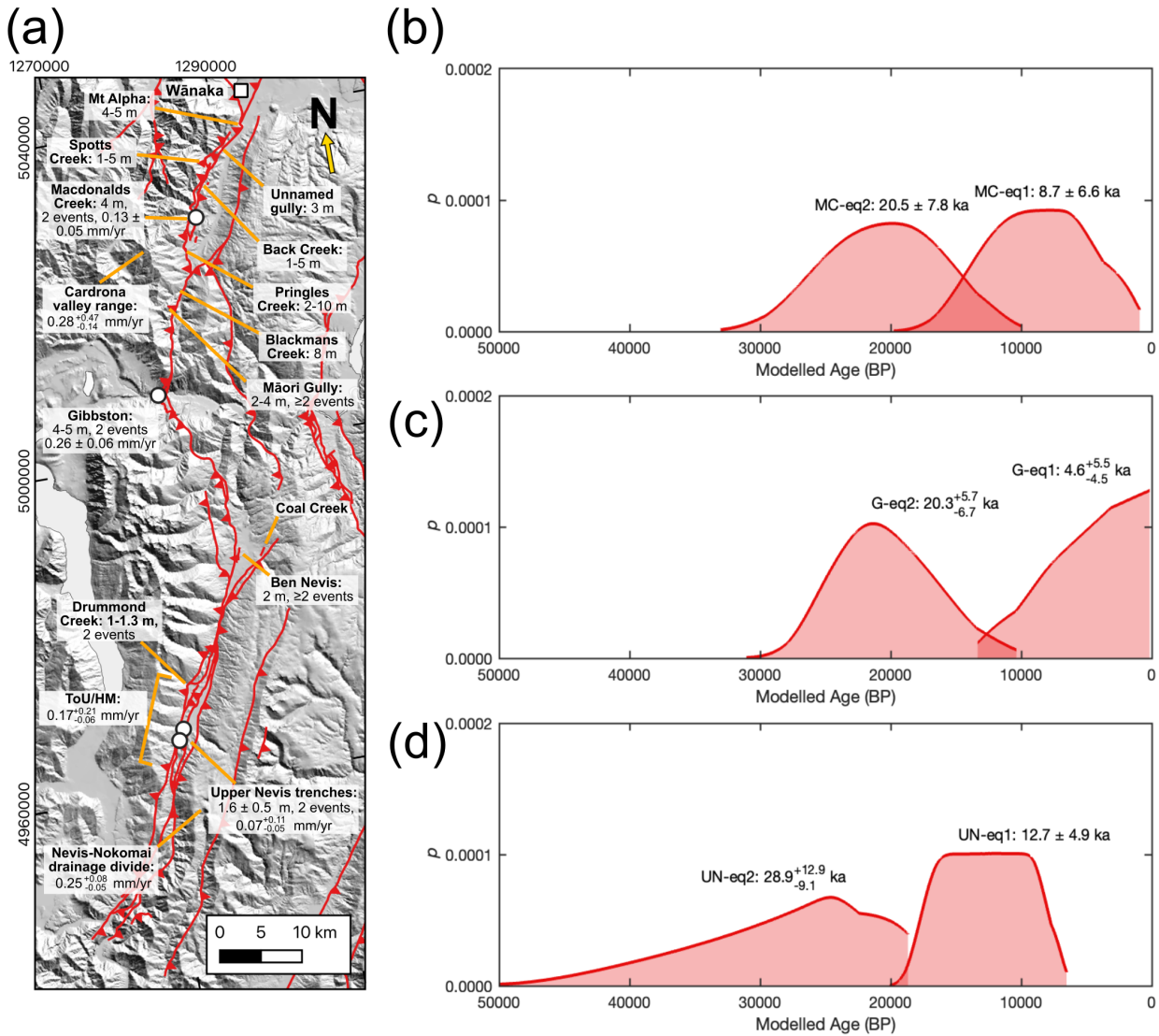


Figure 10 (a) Map of paleoseismic trenches on the NCF and the vertical separation of geomorphic surfaces across its scarps, as collated from this study, [Beanland and Barrow-Hurlbert \(1988\)](#), [van den Berg et al. \(2023\)](#), and [Barrell \(2019\)](#). Where known, the number of surface ruptures that formed these events and the resulting slip rate is indicated (see also Table 4). NCF scarp profiles are also reproduced in Supplementary Information S2. Rupture timing probability distributions for (b) Macdonalds Creek ([van den Berg et al., 2023](#)), (c) Gibbston ([Beanland and Barrow-Hurlbert \(1988\)](#), subsequently revised by [van den Berg et al. \(2023\)](#)) and (d) combined chronology from the German Creek and Stoney Creek trenches (this study). Coordinates in (a) in NZTM. ToU/HM; Tapuae-o-Uenuku/Hector Mountains.

set, we can place a different upper bound slip rate of $0.10^{+0.08}_{-0.05}$ mm/yr (AF1 surface-2, Table 4). Given that the Nevis strand has accommodated all of the most recent NCF displacement in the Upper Nevis valley ([Beanland and Barrow, 1984b](#); [Barrow-Hurlbert, 1985](#)), these revised slip rates ($0.07^{+0.11}_{-0.05}$) are lower than previous estimates for the NCF's Nevis segment (0.4 ± 0.2 mm/yr; [Litchfield et al., 2014](#); [Seebeck et al., 2024](#)).

For a longer-term perspective, a Nevis segment uplift rate of $0.25^{+0.08}_{-0.05}$ mm/yr since 400 ± 100 ka is estimated from the growth of the Nevis-Nokomai river drainage divide, 6 km south of the trenches ('Nevis-Nokomai drainage divide', Table 4, Fig. 10a; [Waters et al., 2001](#)). Alternatively, if we assume that the total height of the Tapuae-o-Uenuku/Hector Mountains above the valley

floor represents the cumulative Nevis segment offset in the Upper Nevis valley (~750 m, Fig. 1d), and that this offset initiated in the Late Miocene-Early Pliocene (4.5 ± 2.5 Ma; [Beanland and Barrow-Hurlbert, 1988](#); [McDonnell and Crow, 2003](#)), then we can estimate an uplift rate of $0.17^{+0.21}_{-0.06}$ mm/yr (Table 4, Fig. 10). An equivalent comparison for the NCF's NW Cardrona segment indicates a late Quaternary uplift rate of 0.12 ± 0.04 mm/yr ([van den Berg et al., 2023](#)) and, given a range height of 1250 ± 250 m above the Cardrona valley floor (Fig. 1d), a $0.28^{+0.5}_{-0.15}$ mm/yr long term uplift rate (Table 4, Fig. 10). These long-term NCF slip rate estimates should be viewed as minimum constraints as they do not consider that some fault offset may be obscured below late Cenozoic sediments in the Cardrona and Upper Nevis

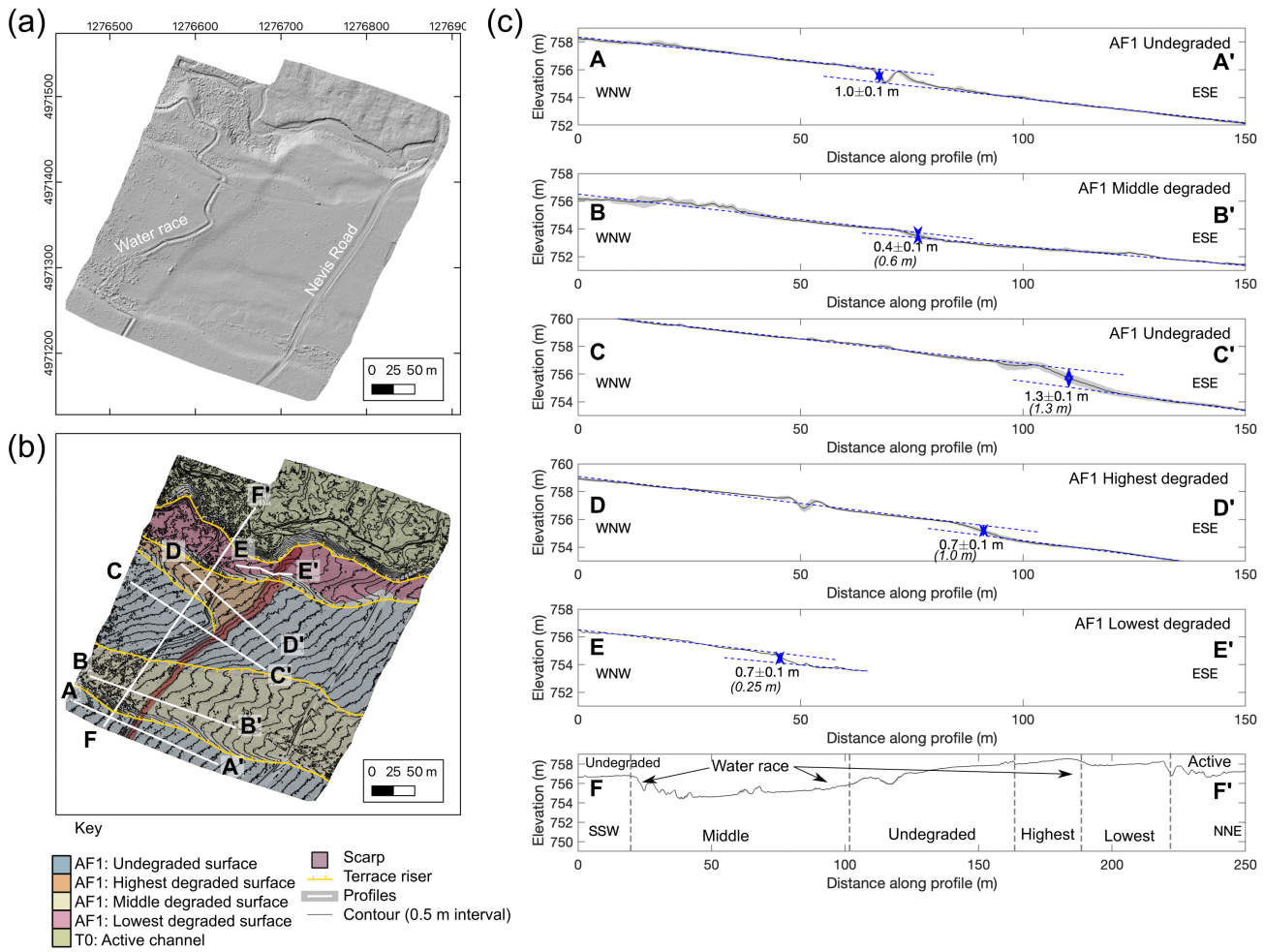


Figure 11 Drummond Creek digital surface model (DSM) without (a) and (b) with geomorphic interpretations. ‘Water race’ indicates artificial channels excavated to control water supply during gold mining in the Nevis valley. (c) Mean (black line) and standard deviation (grey shading) of topographic profiles through the DSM from 20 m wide (15 and 4 m wide for profiles A-A’ and E-E’) swaths centred around lines shown in (b). Profiles are drawn so that they follow the geomorphic surface’s dip direction. The minimal grey shading in the profiles indicates there is little uncertainty in the offset measurements due to lateral variations in displacement or non-planarity of the offset surfaces. We assign a nominal ± 0.1 m uncertainty to the offset measurements to reflect potential errors with how the crest and base of the scarp are picked in the topographic profiles, and with the DSM itself. Numbers in italics indicate the vertical displacement across these scarps measured by [Beanland and Barrow-Hurlbert \(1988\)](#). Coordinates in (a) in NZTM.

valleys. Furthermore, the low preservation of the Wai-pounamu Erosion Surface (WES) west of the NCF ([Turnbull, 2000](#); [Boyce, 2002](#)) indicates some hanging-wall uplift has been removed by erosion. Nevertheless, this uncertainty only serves to support our inference that the NCF slip rate since 50 ka is less than its long term slip rate (Table 4).

East of the NCF, the WES is extensively preserved, and its vertical offset is considered to provide a record of total late Cenozoic fault throw ([Stirling, 1990](#); [Griffin et al., 2022b](#)). Notably, the late Quaternary uplift rates for the Hyde and Akatore faults near the eastern edge of the Otago range and basin reverse fault province (Fig. 1a) are higher than implied by their vertical offset of the WES ([Beanland and Berryman, 1989](#); [Taylor-Silva et al., 2020](#); [Griffin et al., 2022a,b](#)). Under the assumption of constant regional convergent rates, [Griffin et al. \(2022b\)](#) proposed this indicates that deformation

within the Otago range and basin reverse fault province is progressively migrating onto its eastern faults. This suggestion is supported by our finding that the NCF, which lies at the western edge of the Otago reverse fault province, has had a corresponding reduction of slip rate since at least ~ 50 ka. Similar observations of where the boundary conditions imposed by regional deformation rates are constant, but spatial migrations of deformation within the fault network drive interdependent slip rates variations on individual faults, have been documented in other low strain rate regions (e.g., Taupō Rift, Basin and Range Province, central Greece; [Nicol et al., 2006](#); [Pérouse and Wernicke, 2017](#); [Iezzi et al., 2021](#)).

5.2 Along-strike extent of NCF earthquakes

The timings for the most recent rupture in the Upper Nevis, Gibbston, and Macdonalds Creek trenches are only weakly correlated (i.e., UN-eq1 - G-eq1 - MC-eq1,

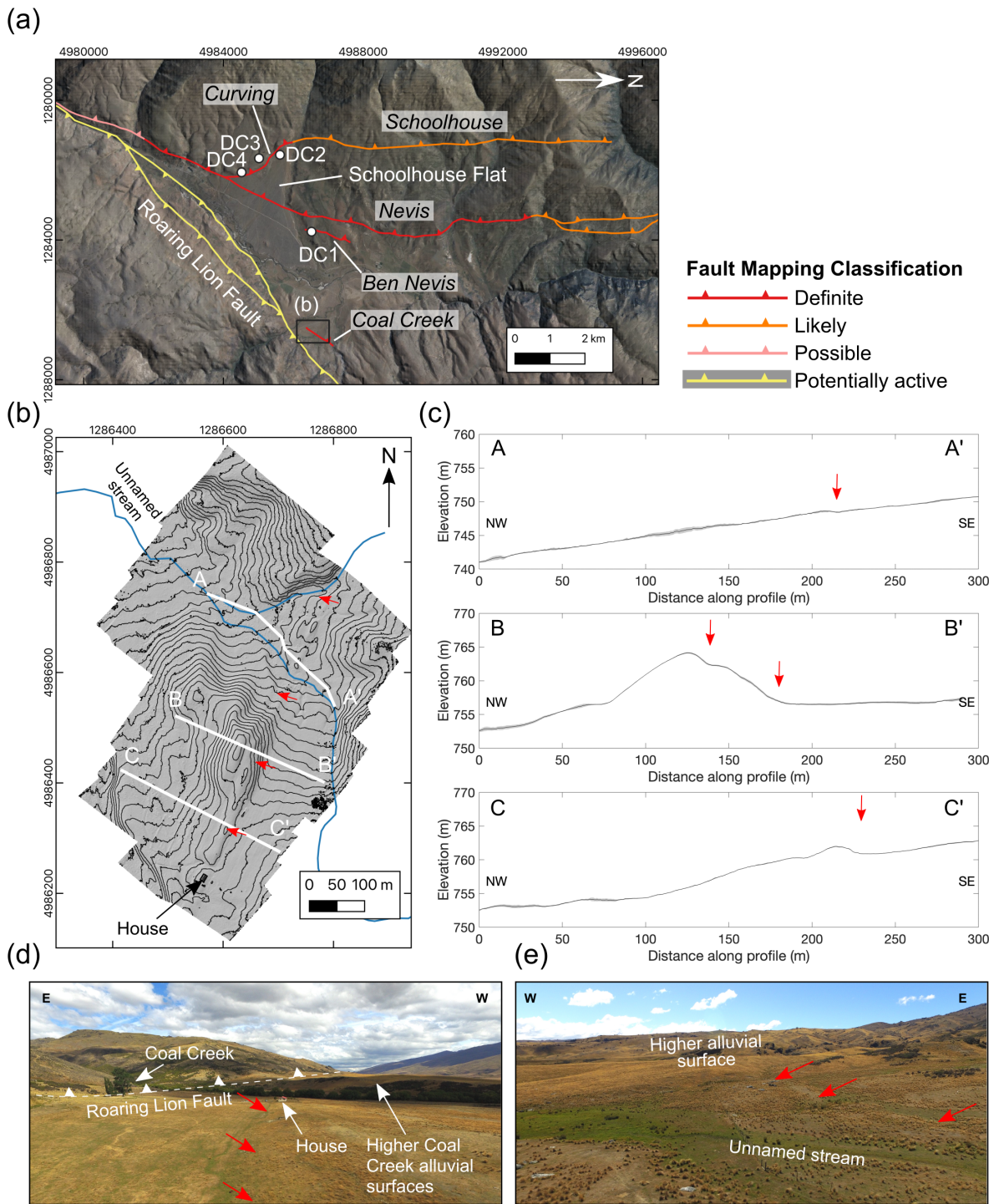


Figure 12 (a) Lower Nevis valley active fault map (Barrell, 2019) and trench locations (Beanland and Barrow-Hurlbert, 1988). Map extent shown in Fig. 1c. Maps underlain by New Zealand 8 m digital elevation model and LINZ Aerial Imagery Basemap. (b) Digital surface model (DSM) of the Coal Creek locality with 1 m interval contours. Red arrows indicate scarp identified by Beanland and Barrow-Hurlbert (1988) and inferred here to be a strike ridge. (c) Mean (black line) and standard deviation (grey shading) of profiles through the Coal Creek DSM created from 20 m wide swaths centred along the lines indicated in (b). Drone photos looking (d) south and (e) north at the Coal Creek locality. A house is labelled in (d) and (b) to indicate their relative positions. Coordinates in a&b in NZTM.

Fig. 10 and Table 3). Hence it is unlikely that the most recent NCF ruptures was a multi-segment event. However, we cannot entirely exclude this possibility using paleoseismic data, as the poorly constrained rupture timings still allow a range of plausible event correlations between these trenches (Table 3). To investigate

the along-strike extent of late Quaternary NCF earthquakes further, we therefore also consider empirical scaling between single event displacement and rupture length (Thingbaijam et al., 2017) for different NCF rupture cases (Table 5).

We estimate a single event displacement (SED) in the

Offset datum	Vertical offset (m)	Age (ka)	Uplift rate (mm/yr)	Slip rate (mm/yr)	Notes
AF1 surface-1	1.4±0.4	47.9±2.2	0.03±0.01	0.04 ^{+0.03} _{-0.02}	minimum constraint
AF1 surface-2	1.4±0.4	20.7±0.8	0.07±0.02	0.10 ^{+0.08} _{-0.05}	maximum constraint
Base of Unit 3 gravels	2.6±0.9	47.9±2.2	0.05 ± 0.02	0.08 ^{+0.07} _{-0.04}	maximum constraint
Nevis-Nokomai drainage divide	100	400±100	0.25 ^{+0.08} _{-0.05}	0.35 ^{+0.32} _{-0.12}	after Waters et al. (2001)
Tapuae-o-Uenuku/Hector Mountains	750	4,500±2,500	0.17 ^{+0.21} _{-0.06}	0.24 ^{+0.51} _{-0.12}	minimum constraint
Macdonalds Creek, NW Cardrona segment	4.0	39.0±14.4	0.12±0.04	0.13±0.05	after van den Berg et al. (2023)
Gibbston, NW Cardrona segment	4.5±0.5	24.7±2.5	0.18±0.04	0.26±0.06	after Beanland and Barrow-Hurlbert (1988)
Cardrona valley range	1250±250	4,500±2,500	0.28 ^{+0.47} _{-0.14}	0.39 ^{+1.11} _{-0.13}	minimum constraint

Table 4 Range of uplift and slip rate estimates for the NCF. Location of estimates along the NCF is provided in Fig. 10. Slip rate estimates derived assuming a $45^\circ \pm 15^\circ$ NCF fault dip (Seebeck et al., 2024), except for the Macdonalds Creek and Gibbston scarps where the fault dips 66° and 45° respectively (Beanland and Barrow-Hurlbert, 1988; van den Berg et al., 2023).

Rupture Case	Length (km)	Thingbaijam et al. (2017)	
		Average SED (m)	M_W
Upper Nevis only	8	0.3 ^{+0.5} _{-0.2}	5.9 ^{+1.1} _{-1.0}
Upper-Lower Nevis	25	0.8 ^{+2.4} _{-0.4}	6.7 ^{+1.2} _{-1.1}
Upper Nevis-Gibbston	45	1.4 ^{+4.9} _{-0.7}	7.1 ^{+1.4} _{-1.1}
Gibbston-Wānaka	40	1.3 ^{+4.2} _{-0.7}	7.0 ^{+1.3} _{-1.1}
Upper Nevis-Wānaka	85	2.7 ^{+10.7} _{-1.4}	7.5 ^{+1.4} _{-1.1}

Table 5 Estimated single event displacement (SED) and M_W for different NCF rupture scenarios given the Thingbaijam et al. (2017) fault scaling.

Upper Nevis valley of $1.0^{+0.7}_{-0.3}$ m by projecting the vertical separation across AF1 at Stoney, German, and Drummond creeks (1.4 ± 0.4 m) through a fault dip of $45^\circ \pm 15^\circ$ and dividing by the two events that we infer to have formed these scarps. It is therefore likely that late Quaternary Nevis segment surface ruptures extended beyond the 8 km long Upper Nevis valley (0.3 m SED, Table 5). Furthermore, compilations of historical earthquakes in Aotearoa New Zealand indicate that a 8 km long $M_W \sim 5.9$ rupture confined to the Upper Nevis valley would have a <10% change of surface rupture (Nicol et al., 2016). No NCF scarps have been identified immediately along-strike to the south of the Upper Nevis valley in the Nokomai River valley (Fig. 1d; Kerr et al., 2000), or to the north along the 10 km long gorge that connects the Upper and Lower Nevis valleys. However, this may simply reflect that there has been extensive landsliding in the steep terrain adjacent to the Upper Nevis valley, and so the chance of scarp preservation there is low.

The closest known NCF scarps to the Upper Nevis valley are on mid- to high-level surfaces in the Lower Nevis valley (Section 4.2.2, Fig. 12a). Notably, the Ben Nevis scarp's vertical offset is 2 m, and given that trench

DC1 provided evidence for ≥ 2 earthquakes (Beanland et al., 1984; Beanland and Barrow-Hurlbert, 1988), the SED in these events must have been $\leq 1.6 \pm 0.4$ m (assuming a fault dip of $45^\circ \pm 15^\circ$). This is comparable to the NCF activity we infer for the Upper Nevis valley, and the fault scaling is compatible with through-going Upper-Lower Nevis valley ruptures (Table 5). Without any chronostratigraphic data to constrain earthquake ages in the Lower Nevis valley, any correlations between it and the Upper Nevis are tentative. If they are true, however, they require that the unfaulted Schoolhouse Flat (Fig. 12a) is younger than the last Nevis segment surface rupture (~ 12 ka, Section 4.1.3), and so this surface is younger than the 'Hawea' (18 ka) age previously assigned to it (Williams, 1974; Beanland and Barrow-Hurlbert, 1988).

NCF scarps have not been identified immediately north of the Lower Nevis valley where it passes through two prominent fault bends between Doolans Saddle and Gibbston (Fig. 1b; Barrell, 2019). However, this region's steep terrain and extensive landsliding is not conducive to scarp preservation. A 45 km long rupture that extended between the Upper Nevis and the prominent NCF scarp at Gibbston is conceivable given the fault-

scaling constraints (Table 5). However, we consider this an unlikely scenario as it implies that the last two surface ruptures at Gibbston did not then propagate further north into the Cardrona valley, and this is inconsistent with: (1) the continuity of scarps with similar height between Gibbston and the Cardrona valley, and (2) well correlated rupture timings between the Gibbston and Macdonalds Creek trenches (Fig. 10; van den Berg et al., 2023). Instead, we infer that if ruptures propagated from the Upper Nevis to Gibbston, then they must have also extended further north in multi-segment NCF ruptures.

For the case of multi-segment NCF ruptures, we consider a 85 km long $M_W \sim 7.5$ rupture that extends from the Upper Nevis valley to the northernmost late Quaternary NCF offsets near Wānaka (Table 5; Barrell, 2019). In this scenario, the expected SED is higher than inferred from the Upper Nevis trenches (2.5–3 m vs. $1.0^{+0.7}_{-0.3}$ m, Table 5). A multi-segment NCF rupture is consistent with, but at the upper range of, SED estimates from the Māori Gully, Gibbston, and Macdonald Creek trenches (2 ± 1 m; Beanland and Barrow-Hurlbert, 1988; van den Berg et al., 2023). Furthermore, the vertical separation of mid-level alluvial surfaces across Cardrona segment scarps (4.5 ± 3.5 m, Fig. 10, Supplementary Information S2; Barrell, 2019; van den Berg et al., 2023) are consistently higher than on the Nevis segment (1.5–2 m). This implies that if multi-segment late Quaternary NCF ruptures did occur they had an asymmetric slip distribution. However, it is generally observed that multi-segment reverse fault earthquake exhibit overall elliptical (or *sinesqrt* function) co-seismic slip profiles (Philip et al., 1992; Yang et al., 2021; Thingbaijam et al., 2022).

In summary, from considering the weak paleoseismic evidence for multi-segment late Quaternary NCF ruptures, the SED-rupture length scaling, and the NCF's along-strike slip distribution, we favour an interpretation of single segment NCF ruptures. In this context, the two surface rupturing earthquakes inferred from the Gibbston and the Macdonalds Creek trench represent ~ 40 km long NW Cardrona segment ruptures between Wānaka and Gibbston $20.5^{+5.0}_{-5.5}$ ka and $6.5^{+4.3}_{-3.7}$ ka (van den Berg et al., 2023). By contrast, the trenches we document here in the Upper Nevis valley record Nevis segment ruptures $28.9^{+12.9}_{-9.1}$ and 12.7 ± 4.9 ka. It is likely that these ruptures extended between the Lower and Upper Nevis valleys, and possibly from the Nokomai catchment to Gibbston. Our interpretation therefore suggests that hard-linked ~ 30 – 50° fault bends by Gibbston and/or Doolans Saddles (Fig. 1) acted as rupture barriers during late Quaternary NCF surface rupturing earthquakes.

6 Conclusions

We document new fault mapping and two paleoseismic trenches along the Nevis-Cardrona Fault (NCF) in the low strain rate Otago range and basin reverse fault province, Aotearoa New Zealand. The trenches were excavated in the Upper Nevis valley on the NCF's Nevis segment, and provide stratigraphic evidence for two surface rupturing earthquakes. From OSL dating and

OxCal modelling we constrain these ruptures to have occurred at $28.9^{+12.9}_{-9.1}$ and 12.7 ± 4.9 ka. By considering either the vertical offset across the NCF scarp (1.4 ± 0.4 m) or the base of alluvial fan gravels (2.6 ± 0.9 m), we estimate slip rates for the Nevis segment of $0.07^{+0.11}_{-0.05}$ mm/yr. These results indicate lower slip rates on the Nevis segment than previous estimates (0.4 ± 0.2 mm/yr; Litchfield et al., 2014; Seebeck et al., 2024).

Comparisons with rupture timings obtained from trench data on the NCF's NW Cardrona segment do not allow us to statistically exclude the possibility that ruptures in the Upper Nevis valley propagated for 85 km along-strike towards Wānaka in multi-segment earthquakes, though the evidence for this is weak. Furthermore, when placed in the context of rupture length-single event displacement scaling, we suggest that NCF hosted single segment ruptures during the late Quaternary. At the regional scale, our results are consistent with previous studies, which indicate that the 1-2 mm/yr of Australian-Pacific plate motion accommodated by the Otago range and basin reverse fault province is currently localised on its easternmost faults.

Acknowledgements

This research was funded by the Toka Tū Ake Natural Hazards Commission University Research Program project 'Understanding and Managing Seismic Risk in Low Seismic Hazard Zone' (RCP-023). Permission to excavate paleoseismic trenches at German Creek and Stoney Creek in the Nevis valley was granted by the leaseholders at Kingston Station, Resource Consent RC210441 from the Central Otago District Council, and a deed of easement from Toitū Te Whenua Land Information New Zealand. We thank the team from Central Excavating for digging the trenches. Permission to fly an Unmanned Aerial Vehicle at Drummond Creek (Remarkables Conservation Area) was permissible through a one-off filming concession from the Department of Conservation Te Papa Atawhai. We also acknowledge the Craigroy Station landowners for permitting access to the Coal Creek locality. We thank David Barrell for providing comments on an earlier version of this manuscript, and Nicholas Harrichhausen and an anonymous reviewer for their insightful and helpful reviews.

Data and code availability

Supplements S1-S4, unannotated orthomosaics of the Stoney and German creek trench walls, and the digital surface models described in Section 3.2 are available at <https://zenodo.org/doi/10.5281/zenodo.10819579>. The New Zealand 8 m digital elevation model and aerial imagery in Figs. 1, 2, 12, and S5 are accessible at <https://data.linz.govt.nz/layer/51768-nz-8m-digital-elevation-model-2012> (last accessed December 21st 2022), and <https://www.linz.govt.nz/data/linz-data/aerial-imagery> (last accessed December 21st 2022), and are provided courtesy of Toitū Te Whenua Land Information New Zealand (LINZ), and licensed by Toitū

Te Whenua LINZ for re-use under the Creative Commons Attribution 4.0 International licence. The New Zealand 80 m digital elevation model in Fig. 1a is available at: <https://koordinates.com/layer/1418-nz-80m-digital-elevation-model/> (last accessed December 21st 2022) under a Creative Commons Attribution 3.0 International licence. The Cardrona valley lidar in Figs. S6-S13 are available at <https://data.linz.govt.nz/layer/99123-otago-lidar-1m-dem-2016/> (last accessed September 18th 2023) and are licensed by Toitū Te Whenua LINZ for re-use under the Creative Commons Attribution 4.0 International licence.

Competing interests

The authors declare they have no competing interests

References

- Accardo, N. J., Shillington, D. J., Gaherty, J. B., Scholz, C. A., Nyblade, A. A., Chindandali, P. R. N., Kamihanda, G., McCartney, T., Wood, D., and Wambura Ferdinand, R. Constraints on Rift Basin Structure and Border Fault Growth in the Northern Malawi Rift From 3-D Seismic Refraction Imaging. *Journal of Geophysical Research: Solid Earth*, 123(11):3–10, 2018. doi: 10.1029/2018JB016504.
- Amos, C. B., Burbank, D. W., and Read, S. A. Along-strike growth of the Ostler fault, New Zealand: Consequences for drainage deflection above active thrusts. *Tectonics*, 29(4), 2010. doi: 10.1029/2009TC002613.
- Angster, S., Wesnousky, S., Huang, W. L., Kent, G., Nakata, T., and Goto, H. Application of UAV photography to refining the slip rate on the Pyramid Lake fault zone, Nevada. *Bulletin of the Seismological Society of America*, 106(2):785–798, 2016. doi: 10.1785/0120150144.
- Arrowsmith, R. J., Crosby, C. J., Korzhonkov, A. M., Mamyrov, E., Povolotskaya, I., Guralnik, B., and Landgraf, A. Surface rupture of the 1911 Kebin (Chon-Kemin) earthquake, Northern Tien Shan, Kyrgyzstan. *Geological Society Special Publication*, 432(1): 233–253, 2017. doi: 10.1144/SP432.10.
- Barnes, P. M. Postglacial (after 20 ka) dextral slip rate of the offshore Alpine fault, New Zealand. *Geology*, 37(1):3–6, 2009. doi: 10.1130/G24764A.1.
- Barrell, D. General distribution and characteristics of active faults and folds in the Queenstown Lakes and Central Otago districts, Otago. *GNS Science, Consultancy Report 2018/207*, pages 1–99, 2019.
- Barrell, D., Litchfield, N., Van Dissen, R., Wang, N., Taylor-Silva, B. I., Hornblow, S., and Stirling, M. Investigation of past earthquakes on the Titri Fault, coastal Otago, New Zealand. *GNS Science, Consultancy Report 2017/35*, pages 1–66, 2020. doi: 10.21420/G2TW6S.
- Barrell, D. J. *Quaternary Glaciers of New Zealand*, volume 15. Elsevier Inc., 1 edition, 2011. doi: 10.1016/B978-0-444-53447-7.00075-1.
- Barrow-Hurlbert, S. A. Geology and neotectonics of the Upper Nevis Basin, South Island, New Zealand. Master's thesis, Oregon State University, 1985. Available at: https://ir.library.oregonstate.edu/concern/graduate_thesis_or_dissertations/ht24wn51t.
- Barth, N. C., Kulhanek, D. K., Beu, A. G., Murray-Wallace, C. V., Hayward, B. W., Mildenhall, D. C., and Lee, D. E. New c. 270 kyr strike-slip and uplift rates for the southern Alpine Fault and implications for the New Zealand plate boundary. *Journal of Structural Geology*, 64:39–52, 2014.
- Beanland, S. Reassessment of late Quaternary fault history using new radiocarbon dates, Kawarau trace, Central Otago. *New Zealand Geological Survey/EDS Immediate Report 85/007 (unpublished file report located at GNS Science, Lower Hutt, NZ)*, 1985.
- Beanland, S. and Barrow, S. Geology of the Upper Nevis basin in relation to active tectonics. *New Zealand Geological Survey/EDS Immediate Report 84/005 (unpublished file report located at GNS Science, Lower Hutt, NZ)*, 1984a.
- Beanland, S. and Barrow, S. A. Quaternary geology and late Quaternary tectonic deformation of the Upper Nevis Basin. *New Zealand Geological Survey/EDS Immediate Report 84/006 (unpublished file report located at GNS Science, Lower Hutt, NZ)*, page 21, 1984b.
- Beanland, S. and Barrow, S. A. Trenching investigations of active faulting in the Upper Nevis Basin, Central Otago. *New Zealand Geological Survey/EDS Immediate Report 84/004 (unpublished file report located at GNS Science, Lower Hutt, NZ)*, 1984c.
- Beanland, S. and Barrow-Hurlbert, S. A. The Nevis-Cardrona Fault System, Central Otago, New Zealand: Late Quaternary tectonics and structural development. *New Zealand Journal of Geology and Geophysics*, 31(3):337–352, 1988. doi: 10.1080/00288306.1988.10417780.
- Beanland, S. and Berryman, K. R. Style and episodicity of late Quaternary activity on the Pisa-Grandview fault zone, Central Otago, New Zealand. *New Zealand Journal of Geology and Geophysics*, 32(4):451–461, 1989. doi: 10.1080/00288306.1989.10427553.
- Beanland, S. and Fellows, D. Late Quaternary tectonic deformation in the Kawarau River area, Central Otago. *New Zealand Geological Survey/EDS Immediate Report 84/019 (unpublished file report located at GNS Science, Lower Hutt, NZ)*, 1984.
- Beanland, S., Fellows, D., and Barrow, S. Late Quaternary Faulting in the Lower Nevis Basin, Central Otago. *New Zealand Geological Survey/EDS Immediate Report 84/018 (unpublished file report located at GNS Science, Lower Hutt, NZ)*, 1984.
- Beanland, S., Berryman, K. R., Hull, A., and Wood, P. Late Quaternary deformation at the Dunstan fault, Central Otago, New Zealand. *Roy. Soc. New Zealand Bull.*, 24:293–306, 1986.
- Beanland, S. A. Late Quaternary Faulting in the Cardrona Valley, Central Otago. *New Zealand Geological Survey/EDS Immediate Report 84/017 (unpublished file report located at GNS Science, Lower Hutt, NZ)*, 1984.
- Beavan, J., Wallace, L. M., Palmer, N., Denys, P., Ellis, S., Fournier, N., Hreinsdottir, S., Pearson, C., and Denham, M. New Zealand GPS velocity field: 1995–2013. *New Zealand Journal of Geology and Geophysics*, 59(1):5–14, 2016. doi: 10.1080/00288306.2015.1112817.
- Bell, D. H. Geomorphic evolution of a valley system: the Kawarau Valley, Central Otago. In *Landforms of New Zealand Second Edition*, pages 456–481. Longman Paul Auckland, 1992.
- Biasi, G. P. and Wesnousky, S. G. Steps and gaps in ground ruptures: Empirical bounds on rupture propagation. *Bulletin of the Seismological Society of America*, 106(3):1110–1124, 2016. doi: 10.1785/0120150175.
- Biasi, G. P. and Wesnousky, S. G. Bends and Ends of Surface Ruptures. *Bulletin of the Seismological Society of America*, 107(6): 2543–2560, 2017. doi: 10.1785/0120160292.
- Boyce, Z. L. The Geology and Evolution of the Upper Nevis Basin. Master's thesis, University of Otago, 2002. Available at: <http://theses.otagogeology.org.nz/items/show/392>.

- Bronk Ramsey, C. Bayesian analysis of radiocarbon dates. *Radiocarbon*, 51(1):337–360, 2009. doi: 10.1017/s0033822200033865.
- Carretier, S., Ritz, J. F., Jackson, J., and Bayasgalan, A. Morphological dating of cumulative reverse fault scarps: Examples from the Gurvan Bogd fault system, Mongolia. *Geophysical Journal International*, 148(2):256–277, 2002. doi: 10.1046/j.1365-246X.2002.01599.x.
- Cartwright, J. A., Trudgill, B. D., and Mansfield, C. S. Fault growth by segment linkage: an explanation for scatter in maximum displacement and trace length data from the Canyonlands Grabens of SE Utah. *Journal of Structural Geology*, 17(9):1319–1326, 1995. doi: 10.1016/0191-8141(95)00033-A.
- Chartier, T., Scotti, O., and Lyon-Caen, H. Sherifs: Open-source code for computing earthquake rates in fault systems and constructing hazard models. *Seismological Research Letters*, 90(4):1678–1688, 2019. doi: 10.1785/0220180332.
- Chiama, K., Chauvin, B., Plesch, A., Moss, R., and Shaw, J. H. Geomechanical Modeling of Ground Surface Deformation Associated with Thrust and Reverse-Fault Earthquakes: A Distinct Element Approach. *Bulletin of the Seismological Society of America*, 113(4):1702–1723, 2023. doi: 10.1785/0120220264.
- Craw, D. River drainage reorientation during placer gold accumulation, southern New Zealand. *Mineralium Deposita*, 48(7):841–860, 2013. doi: 10.1007/s00126-013-0464-5.
- Craw, D., Upton, P., Walcott, R., Burridge, C., and Waters, J. Tectonic controls on the evolution of the Clutha River catchment, New Zealand. *New Zealand Journal of Geology and Geophysics*, 55(4):345–359, 2012. doi: 10.1080/00288306.2012.709184.
- Crone, A. J. and Haller, K. M. Segmentation and the coseismic behavior of Basin and Range normal faults: examples from east-central Idaho and southwestern Montana, U.S.A. *Journal of Structural Geology*, 13(2):151–165, 1991. doi: https://doi.org/10.1016/0191-8141(91)90063-0.
- Dawers, N. H. and Anders, M. H. Displacement-length scaling and fault linkage. *Journal of Structural Geology*, 17(5):607–614, 1995. doi: 10.1016/0191-8141(94)00091-D.
- Denys, P., Pearson, C., Norris, R., and Denham, M. A geodetic study of Otago: results of the central Otago deformation network 2004–2014. *New Zealand Journal of Geology and Geophysics*, 59(1):147–156, 2016. doi: 10.1080/00288306.2015.1134592.
- Douilly, R., Aochi, H., Calais, E., and Freed, A. M. Three-dimensional dynamic rupture simulations across interacting faults: The Mw 7.0, 2010, Haiti earthquake. *Journal of Geophysical Research: Solid Earth*, 120(2):1108–1128, 2015. doi: 10.1002/2014JB011595.
- DuRoss, C. B., Personius, S. F., Crone, A. J., Olig, S. S., and Lund, W. R. Integration of paleoseismic data from multiple sites to develop an objective earthquake chronology: Application to the Weber segment of the Wasatch fault zone, Utah. *Bulletin of the Seismological Society of America*, 101(6):2765–2781, 2011. doi: 10.1785/0120110102.
- DuRoss, C. B., Personius, S. F., Crone, A. J., Olig, S. S., Hylland, M. D., Lund, W. R., and Schwartz, D. P. Fault segmentation: New concepts from the Wasatch Fault Zone, Utah, USA. *Journal of Geophysical Research: Solid Earth*, 121(2):1131–1157, 2016. doi: 10.1002/2015JB012519.
- Eberhart-Phillips, D., Upton, P., Reyners, M., Barrell, D. J., Fry, B., Bourguignon, S., and Warren-Smith, E. The Influence of Basement Terranes on Tectonic Deformation: Joint Earthquake Travel-Time and Ambient Noise Tomography of the Southern South Island, New Zealand. *Tectonics*, 41(4):e2021TC007006, 2022. doi: 10.1029/2021TC007006.
- Ellis, M. A. and Dunlap, W. J. Displacement variation along thrust faults: implications for the development of large faults. *Journal of Structural Geology*, 10(2):183–192, 1988. doi: 10.1016/0191-8141(88)90115-0.
- Faure Walker, J., Boncio, P., Pace, B., Roberts, G., Benedetti, L., Scotti, O., Visini, F., and Peruzza, L. Fault2SHA Central Apennines database and structuring active fault data for seismic hazard assessment. *Scientific Data*, 8(1):1–20, 2021. doi: 10.1038/s41597-021-00868-0.
- Field, E. H., Arrowsmith, R. J., Biasi, G. P., Bird, P., Dawson, T. E., Felzer, K. R., Jackson, D. D., Johnson, K. M., Jordan, T. H., Madden, C., Michael, A. J., Milner, K. R., Page, M. T., Parsons, T., Powers, P. M., Shaw, B. E., Thatcher, W. R., Weldon, R. J., and Zeng, Y. Uniform California Earthquake Rupture Forecast, version 3 (UCERF3) -The time-independent model. *Bulletin of the Seismological Society of America*, 104(3):1122–1180, 2014. doi: 10.1785/0120130164.
- Font, M., Lagarde, J.-L., Amorese, D., Coutard, J.-P., Dubois, A., Guillemet, G., Ozouf, J.-C., and Vedie, E. Physical modelling of fault scarp degradation under freeze–thaw cycles. *Earth Surface Processes and Landforms*, 31(14):1731–1745, 2006. doi: https://doi.org/10.1002/esp.1371.
- Gerstenberger, M. C., Van Dissen, R., Rollins, C., Dicaprio, C., Thingbaijim, K. K., Bora, S., Chamberlain, C., Christophersen, A., Coffey, G. L., Ellis, S. M., Iturrieta, P., Johnson, K. M., Litchfield, N. J., Nicol, A., Milner, K. R., Rastin, S. J., Rhoades, D., Seebeck, H., Shaw, B. E., Stirling, M. W., Wallace, L., Allen, T. I., Bradley, B. A., Charlton, D., Clark, K. J., Fraser, J., Griffin, J., Hamling, I. J., Howell, A., Hudson-Doyle, E., Hulsey, A., Jurgens, V. O., Kaiser, A. E., Kirkman, R., Langridge, R. M., Maurer, J., Rattenbury, M. S., Ristau, J., Schorlemmer, D., Townend, J., Villamor, P., and Williams, C. The Seismicity Rate Model for the 2022 Aotearoa New Zealand National Seismic Hazard Model. *Bulletin of the Seismological Society of America*, 114(1):182–216, 2024. doi: 10.1785/0120230165.
- Griffin, J. D., Stirling, M. W., Barrell, D. J., van den Berg, E. J., Todd, E. K., Nicolls, R., and Wang, N. Paleoseismology of the Hyde Fault, Otago, New Zealand. *New Zealand Journal of Geology and Geophysics*, 65(4):613–637, 2022a. doi: 10.1080/00288306.2021.1995007.
- Griffin, J. D., Stirling, M. W., Wilcken, K. M., and Barrell, D. J. Late Quaternary slip rates for the Hyde and Dunstan faults, southern New Zealand: implications for strain migration in a slowly deforming continental plate margin. *Tectonics*, 41(9):e2022TC007250, 2022b. doi: 10.1029/2022TC007250.
- Heron, D. W. NZL GNS 1:1M geology. 2nd edition [Data set]. Technical report, GNS Science, 2014.
- Hogg, A. G., Heaton, T. J., Hua, Q., Palmer, J. G., Turney, C. S., Southon, J., Bayliss, A., Blackwell, P. G., Boswijk, G., Bronk Ramsey, C., Pearson, C., Petchey, F., Reimer, P., Reimer, R., and Wacker, L. SHCal20 Southern Hemisphere Calibration, 0–55,000 Years cal BP. *Radiocarbon*, 62(4):759–778, 2020. doi: 10.1017/RDC.2020.59.
- Hubbard, J., Shaw, J. H., Dolan, J., Pratt, T. L., McAuliffe, L., and Rockwell, T. K. Structure and seismic hazard of the Ventura Avenue anticline and ventura fault, California: Prospect for large, multisegment ruptures in the western transverse ranges. *Bulletin of the Seismological Society of America*, 104(3):1070–1087, 2014. doi: 10.1785/0120130125.
- Iezzi, F., Roberts, G., Faure Walker, J., Papanikolaou, I., Ganas, A., Deligiannakis, G., Beck, J., Wolfers, S., and Gheorghiu, D. Temporal and spatial earthquake clustering revealed through comparison of millennial strain-rates from ³⁶Cl cosmogenic exposure dating and decadal GPS strain-rate. *Scientific Reports*, 11(1), 2021. doi: 10.1038/s41598-021-02131-3.
- Jackson, J., Norris, R., and Youngson, J. The structural evolution of

- active fault and fold systems in central Otago, New Zealand: Evidence revealed by drainage patterns. *Journal of Structural Geology*, 18(2-3):217–234, 1996. doi: 10.1016/S0191-8141(96)80046-0.
- Johnson, K., Nissen, E., Saripalli, S., Arrowsmith, J. R., McGarey, P., Scharer, K., Williams, P., and Blisniuk, K. Rapid mapping of ultrafine fault zone topography with structure from motion. *Geosphere*, 10(5):969–986, 2014. doi: 10.1130/GES01017.1.
- Johnson, K. M., Wallace, L. M., Maurer, J., Hamling, I., Williams, C., Rollins, C., Gerstenberger, M., and Van Dissen, R. Inverting Geodetic Strain Rates for Slip Deficit Rate in Complex Deforming Zones: An Application to the New Zealand Plate Boundary. *Journal of Geophysical Research: Solid Earth*, 129(3):e2023JB027565, 2024. doi: 10.1029/2023JB027565.
- Kalacska, M., Lucanus, O., Arroyo-Mora, J. P., Laliberté, É., Elmer, K., Leblanc, G., and Groves, A. Accuracy of 3d landscape reconstruction without ground control points using different uas platforms. *Drones*, 4(2):1–26, 2020. doi: 10.3390/drones4020013.
- Kerr, L. C., Craw, D., Norris, R. J., Youngson, J. H., and Wopereis, P. Structure, geomorphology, and gold concentration in the Nokomai valley, Southland, New Zealand. *New Zealand Journal of Geology and Geophysics*, 43(3):425–433, 2000. doi: 10.1080/00288306.2000.9514899.
- King, G. C. P. Speculations on the geometry of the initiation and termination processes of earthquake rupture and its relation to morphology and geological structure. *Pure and Applied Geophysics*, 124(3):567–585, 1986. doi: 10.1007/BF00877216.
- Landis, C. A., Campbell, H. J., Begg, J. G., Mildenhall, D. C., Pateron, A. M., and Trewick, S. A. The Waipounamu Erosion Surface: Questioning the antiquity of the New Zealand land surface and terrestrial fauna and flora. *Geological Magazine*, 145(2):173–197, 2008. doi: 10.1017/S0016756807004268.
- Langridge, R. M., Ries, W. F., Litchfield, N. J., Villamor, P., Van Dissen, R. J., Barrell, D. J. A., Rattenbury, M. S., Heron, D. W., Haubrock, S., Townsend, D. B., Lee, J. M., Berryman, K. R., Nicol, A., Cox, S. C., and Stirling, M. W. The New Zealand Active Faults Database. *New Zealand Journal of Geology and Geophysics*, 59(1):86–96, 2016. doi: 10.1080/00288306.2015.1112818.
- Lienkaemper, J. J. and Bronk Ramsey, C. OxCal: Versatile tool for developing paleoearthquake chronologies- A primer. *Seismological Research Letters*, 80(3):431–434, 2009. doi: 10.1785/gssrl.80.3.431.
- Litchfield, N. J., Van Dissen, R., Sutherland, R., Barnes, P. M., Cox, S. C., Norris, R., Beavan, R. J., Langridge, R., Villamor, P., Berryman, K., Stirling, M., Nicol, A., Nodder, S., Lamarche, G., Barrell, D. J. A., Pettinga, J. R., Little, T., Pondard, N., Mountjoy, J. J., and Clark, K. A model of active faulting in New Zealand. *New Zealand Journal of Geology and Geophysics*, 57(1):32–56, 2014. doi: 10.1080/00288306.2013.854256.
- Macara, G. The climate and weather of Otago. *NIWA Science and Technology Series*, 67:44, 2015.
- Mackey, B. Seismic hazard in the Queenstown Lakes district. Technical Report August, Otago Regional Council, 2015.
- Mazzoli, S., Pierantoni, P. P., Borraccini, F., Paltrinieri, W., and Deiana, G. Geometry, segmentation pattern and displacement variations along a major Apennine thrust zone, central Italy. *Journal of Structural Geology*, 27(11):1940–1953, 2005. doi: 10.1016/j.jsg.2005.06.002.
- McCalpin, J. P. and Carver, G. A. Paleoseismology of compressional tectonic environments. *International Geophysics*, 95:315–419, 2009. doi: 10.1016/S0074-6142(09)95005-7 315.
- McDonnell, M. and Craw, D. Stratigraphy and provenance of Pliocene greywacke-bearing conglomerate, Cardrona valley, Otago, New Zealand. *New Zealand Journal of Geology and Geophysics*, 46(3):425–436, 2003. doi: 10.1080/00288306.2003.9515018.
- McKay, A. *Report on the older auriferous drifts of Central Otago*. J. Mackay, government printer, 1897.
- McSaveney, M. J. and Stirling, M. W. Central Otago: Basin and Range country. *Landforms of New Zealand*, pages 482–504, 1992.
- Murray, A. S. and Wintle, A. G. Luminescence dating of quartz using an improved single-aliquot regenerative-dose protocol. *Radiation Measurements*, 32(1):57–73, 2000. doi: 10.1016/S1350-4487(99)00253-X.
- Nicol, A., Walsh, J., Berryman, K., and Villamor, P. Interdependence of fault displacement rates and paleoearthquakes in an active rift. *Geology*, 34(10):865–868, 2006. doi: 10.1130/G22335.1.
- Nicol, A., Van Dissen, R. J., Stirling, M. W., and Gerstenberger, M. C. Completeness of the Paleoseismic Active-Fault Record in New Zealand. *Seismological Research Letters*, 87(6):1299–1310, 2016. doi: 10.1785/0220160088.
- Norris, R. J. Strain localisation within ductile shear zones beneath active faults: The Alpine Fault contrasted with the adjacent Otago fault system, New Zealand. *Earth, Planets and Space*, 56(12):1095–1101, 2004. doi: 10.1186/BF03353328.
- Norris, R. J. and Cooper, A. F. Late Quaternary slip rates and slip-partitioning on the Alpine Fault, New Zealand. *Journal of Structural Geology*, 23(2000):507–520, 2001.
- Pace, B., Stirling, M. W., Litchfield, N. J., and Rieser, U. New active fault data and seismic hazard estimates for west Otago, New Zealand. *New Zealand Journal of Geology and Geophysics*, 48(1):75–83, 2005. doi: 10.1080/00288306.2005.9515099.
- Patyniak, M., Landgraf, A., Dzhumabaeva, A., Baikulov, S., Williams, A. M., Weiss, J. R., Hilley, G. E., Preusser, F., Abdrakhmatov, K. E., Arrowsmith, R. J., and Strecker, M. R. The Pamir Frontal Thrust Fault: Holocene Full-Segment Ruptures and Implications for Complex Segment Interactions in a Continental Collision Zone. *Journal of Geophysical Research: Solid Earth*, 126(12), 2021. doi: 10.1029/2021JB022405.
- Pérouse, E. and Wernicke, B. P. Spatiotemporal evolution of fault slip rates in deforming continents: The case of the Great Basin region, northern Basin and Range province. *Geosphere*, 13(1):112–135, 2017. doi: 10.1130/GES01295.1.
- Philip, H., Rogozhin, E., Cisternas, A., Bousquet, J. C., Borisov, B., and Karakhanian, A. The Armenian earthquake of 1988 December 7: faulting and folding, neotectonics and palaeoseismicity. *Geophysical Journal International*, 110(1):141–158, 1992. doi: 10.1111/j.1365-246X.1992.tb00718.x.
- Rollins, C., Thingbaijam, K. K., Hutson, R., Gerstenberger, M., Christophersen, A., Eberhart-Phillips, D., Rastin, S. J., and Van Dissen, R. An augmented New Zealand earthquake catalogue, event classifications, and models of the depth distribution of shallow earthquakes in the greater New Zealand region. *GNS Science. GNS Science report; 2021/58*, page 83, 2022. doi: 10.21420/XT4Y-WY45.
- Rotevatn, A., Jackson, C. A. L., Tvedt, A. B. M., Bell, R. E., and Blækkann, I. How do normal faults grow? *Journal of Structural Geology*, 125:174–184, 2019. doi: 10.1016/j.jsg.2018.08.005.
- Rubin, C. M. Systematic underestimation of earthquake magnitudes from large intracontinental reverse faults: Historical ruptures break across segment boundaries. *Geology*, 24(11):989–992, 1996. doi: 10.1130/0091-7613(1996)024<0989:SUOEMF>2.3.CO;2.
- Schwanghart, W. and Scherler, D. Short Communication: Topo-Toolbox 2 - MATLAB-based software for topographic analysis and modeling in Earth surface sciences. *Earth Surface Dynam-*

- ics, 2(1):1–7, 2014. doi: 10.5194/esurf-2-1-2014.
- Seebeck, H., Dissen, R. V., Litchfield, N., Barnes, P. M., Nicol, A., Langridge, R., Barrell, D. J., Villamor, P., Ellis, S., Rattenbury, M., Bannister, S., Gerstenberger, M., Ghisetti, F., Sutherland, R., Hirschberg, H., Fraser, J., Nodder, S. D., Stirling, M., Humphrey, J., Bland, K. J., Howell, A., Mountjoy, J., Moon, V., Stahl, T., Spinardi, F., Townsend, D., Clark, K., Hamling, I., Cox, S., de Lange, W., Wopereis, P., Johnston, M., Morgenstern, R., Coffey, G., Eccles, J. D., Little, T., Fry, B., Griffin, J., Townend, J., Mortimer, N., Alcaraz, S., Massiot, C., Rowland, J. V., Muirhead, J., Upton, P., and Lee, J. The New Zealand Community Fault Model–version 1.0: an improved geological foundation for seismic hazard modelling. *New Zealand Journal of Geology and Geophysics*, 67((2)):209–229, 2024. doi: 10.1080/00288306.2023.2181362.
- Stahl, T., Quigley, M. C., and Bebbington, M. S. Tectonic geomorphology of the Fox Peak and Forest Creek Faults, South Canterbury, New Zealand: slip rates, segmentation and earthquake magnitudes. *New Zealand Journal of Geology and Geophysics*, 59(4):568–591, 2016. doi: 10.1080/00288306.2016.1212908.
- Stirling, M. W. The Old Man Range and Garvie Mountains: Tectonic geomorphology of the Central Otago peneplain, New Zealand. *New Zealand Journal of Geology and Geophysics*, 33(2):233–243, 1990. doi: 10.1080/00288306.1990.10425681.
- Styron, R. The impact of earthquake cycle variability on neotectonic and paleoseismic slip rate estimates. *Solid Earth*, 10(1): 15–25, 2019. doi: 10.5194/se-10-15-2019.
- Taylor-Silva, B. I., Stirling, M. W., Litchfield, N. J., Griffin, J. D., van den Berg, E. J., and Wang, N. Paleoseismology of the Akatore Fault, Otago, New Zealand. *New Zealand Journal of Geology and Geophysics*, 63(2):151–167, 2020. doi: 10.1080/00288306.2019.1645706.
- Thingbaijam, K. K., Van Dissen, R., Shaw, B. E., and Gerstenberger, M. Average Coseismic Slip Profiles. *GNS Science report 2021/24*, pages 1–33, 2022. doi:10.21420/S6ED-JN06.
- Thingbaijam, K. K. S., Mai, P. M., and Goda, K. New empirical earthquake source-scaling laws. *Bulletin of the Seismological Society of America*, 107(5):2225–2246, 2017. doi: 10.1785/0120170017.
- Todd, E. K., Stirling, M. W., Fry, B., Salichon, J., and Villamor, P. Characterising microseismicity in a low seismicity region: applications of short-term broadband seismic arrays in Dunedin, New Zealand. *New Zealand Journal of Geology and Geophysics*, 63(3):331–341, 2020. doi: 10.1080/00288306.2019.1707238.
- Turnbull, I. M. Geology of the Wakatipu area, 2000.
- Valentini, A., Visini, F., and Pace, B. Integrating faults and past earthquakes into a probabilistic seismic hazard model for peninsular Italy. *Natural Hazards and Earth System Sciences*, 17(11):2017–2039, 2017. doi: 10.5194/nhess-17-2017-2017.
- Valentini, A., DuRoss, C. B., Field, E. H., Gold, R. D., Briggs, R. W., Visini, F., and Pace, B. Relaxing Segmentation on the Wasatch Fault Zone: Impact on Seismic Hazard. *Bulletin of the Seismological Society of America*, 110(1):83–109, 2020. doi: 10.1785/0120190088.
- van den Berg, E. Paleoseismology of the NW Cardrona Fault, Central Otago. Master's thesis, University of Otago, 2020. Available at: <http://hdl.handle.net/10523/10474>.
- van den Berg, E. J., Williams, J. N., Stirling, M. W., Barrell, D. J., Griffin, J. D., Litchfield, N. J., and Wang, N. Late Quaternary activity of the NW Cardrona Fault, Otago, New Zealand. *New Zealand Journal of Geology and Geophysics*, pages 1–21, 2023. doi: 10.1080/00288306.2023.2297962.
- Van Dissen, R., Barrell, D., Langridge, R., Litchfield, N., Villamor, P., and Tonkin, P. Reassessment of seismic hazard at the Clyde Dam, Central Otago: Earthquake geology field investigations and determination of Dunstan Fault rupture characteristics. *Lower Hutt (NZ). GNS Science Consultancy Report 2006/147.*, 2007.
- Visini, F., Valentini, A., Chartier, T., Scotti, O., and Pace, B. Computational Tools for Relaxing the Fault Segmentation in Probabilistic Seismic Hazard Modelling in Complex Fault Systems. *Pure and Applied Geophysics*, 177(5):1855–1877, 2020. doi: 10.1007/s00024-019-02114-6.
- Walsh, J. J., Bailey, W. R., Childs, C., Nicol, A., and Bonson, C. G. Formation of segmented normal faults: A 3-D perspective. *Journal of Structural Geology*, 25(8):1251–1262, 2003. doi: 10.1016/S0191-8141(02)00161-X.
- Warren-Smith, E., Lamb, S., Stern, T. A., and Smith, E. Microseismicity in Southern South Island, New Zealand: Implications for the Mechanism of Crustal Deformation Adjacent to a Major Continental Transform. *Journal of Geophysical Research: Solid Earth*, 122(11):9208–9227, 2017. doi: 10.1002/2017JB014732.
- Waters, J. M., Craw, D., Youngson, J. H., and Wallis, G. P. Genes meet geology: Fish phylogeographic pattern reflects ancient, rather than modern, drainage connections. *Evolution*, 55(9): 1844–1851, 2001. doi: 10.1111/j.0014-3820.2001.tb00833.x.
- Williams, G. J. Cenozoic geology of the lower Nevis basin, with special reference to shale deposits. *Department of Scientific and Industrial Research Bulletin: Wellington, New Zealand*, 1974.
- Williams, J. N., Werner, M. J., Goda, K., Wedmore, L. N. J., De Risi, R., Biggs, J., Mdala, H., Dulanya, Z., Fagereng, Å., Mphepo, F., and Chindandali, P. Fault-based probabilistic seismic hazard analysis in regions with low strain rates and a thick seismogenic layer: a case study from Malawi. *Geophysical Journal International*, 233(3):2172–2206, 2023. doi: 10.1093/gji/ggad060.
- Yang, H., Quigley, M., and King, T. Surface slip distributions and geometric complexity of intraplate reverse-faulting earthquakes. *Bulletin of the Geological Society of America*, 133(9-10): 1909–1929, 2021. doi: 10.1130/B35809.1.
- Youngson, J. H., Craw, D., Landis, C. A., and Schmitt, K. R. Redefinition and interpretation of late Miocene-Pleistocene terrestrial stratigraphy, Central Otago, New Zealand. *New Zealand Journal of Geology and Geophysics*, 41(1):51–68, 1998. doi: 10.1080/00288306.1998.9514790.
- Youngson, J. H., Wopereis, P., Kerr, L. C., and Craw, D. Au-Ag-Hg and Au-Ag alloys in Nokomai and Nevis valley placers, northern Southland and Central Otago, New Zealand, and their implications for placer-source relationship. *New Zealand Journal of Geology and Geophysics*, 45(1):53–69, 2002. doi: 10.1080/00288306.2002.9514959.
- Zielke, O. and Mai, P. M. MCQsim: A Multicycle Earthquake Simulator. *Bulletin of the Seismological Society of America*, 113(3): 889–908, 2023. doi: 10.1785/0120220248.

The article *Along-strike extent of earthquakes on multi-segment reverse faults; insights from the Nevis-Cardrona Fault, Aotearoa New Zealand* © 2024 by Jack N. Williams is licensed by His Majesty the King in Right of Canada, as represented by the Minister of Natural Resources. Non-Commercial Reproduction. Permission to reproduce Government of Canada works, in part or in whole, and by any means, for personal or public non-commercial purposes, or for cost-recovery purposes, is not required, unless otherwise specified in the material you wish to reproduce. Please see NRCan's terms of use for commercial reproduction: <https://natural-resources.canada.ca/terms-and-conditions/10847>.